

ALMA MATER STUDIORUM - UNIVERSITÀ DI BOLOGNA

SCUOLA DI INGEGNERIA E ARCHITETTURA

*DIPARTIMENTO DI INGEGNERIA CIVILE, CHIMICA, AMBIENTALE E DEI
MATERIALI*

*CORSO DI LAUREA MAGISTRALE IN INGEGNERIA PER L'AMBIENTE E IL
TERRITORIO*

TESI DI LAUREA

in

Opere in Sotterraneo M

**Effects of settlements on Pombalino buildings (Lisbon) taking into
account soil-structure interaction**

CANDIDATO:
Giacomo Rigon

RELATORE:
Prof.ssa Ing. Daniela Boldini

CORRELATORE:
Prof. Ing. Rui Carrilho Gomes

Anno Accademico 2017/2018

Sessione III

Abstract

Failures and damages to infrastructures and buildings may occur near an excavation. One of the causes is the lowering of the water level, which is necessary to perform the excavation or to maintain service. Nowadays the development of underground infrastructures requires a careful analysis of the soil- structure interaction in order to preserve the structures' integrity. This analysis acquires a peculiar relevance when the excavation is done in densely occupied areas or near old buildings. This thesis, developed at Instituto Superior Técnico (IST), presents the case of the Pombalino building in the downtown of Lisbon which, in the last years, has seen an increase in the construction of underground structures. The Pombalino, constructed in the second half of the XVII century, is the symbol of the city's reconstruction after the 1755's earthquake. It is characterized by the Pombalino cage, a wooden structure installed to resist the seismic action; however nowadays this structure has become an element of weakness in the masonry. The work of the thesis aims to analyze the interaction between the soil and the Pombalino building when in the nearby area a drawdown of water level is carried out . The analysis is conducted with the finite element code PLAXIS 2D and focuses on the assessment of the movements under the Pombalino building and on the deformations induced on the facade of the building. The Pombalino cage is simulated thanks to the Jointed Masonry constitutive model, which allows to simulate the weaknesses' directions defined by the wooden beams and enables to quantify the deformations entity.

Keywords

Water drawdown, displacements, excavation, finite element, PLAXIS;

Resumo

Na vizinhança de uma escavação pode ocorrer deformações excessivas em infraestruturas e construções. Uma das causas é o rebaixamento do nível freático necessário para realizar a escavação ou durante a fase de serviço. Hoje em dia, a criação de estruturas subterrâneas exige uma cuidadosa análise sobre a interação terreno-estrutura, a fim de salvaguardar a integridade da estrutura. Esta análise torna-se fundamental quando a escavação é feita em áreas densamente ocupadas ou na presença de edifícios antigos. Esta tese analisa o caso do um edifício pombalino do centro histórico de Lisboa onde, nos últimos anos, se tem desenvolvido a construção de estruturas subterrâneas. O edifício Pombalino, que remonta à segunda metade do século XVIII, representa o símbolo da reconstrução da cidade após o sismo do ano 1755, e caracteriza-se pela presença da gaiola pombalina, uma estrutura de madeira criada naquela altura para resistir à actividade sísmica, que hoje torna-se elemento de fraqueza da alvenaria devido à sua degradação. Este trabalho analisa a interação entre o terreno e o edifício pombalino quando nas proximidades é efectuada o rebaixamento do nível freático. A análise é efectuada através do programa PLAXIS 2D e concentra-se na determinação dos assentamentos do edifício pombalino e nas deformações induzidas na fachada do prédio. A gaiola pombalina é simulada através do modelo numérico Joint Masonry que permite simular as direcções de fraqueza determinadas pelas vigas de madeira, e permite avaliar os danos no edifício.

Palavras Chave

Rebaixamento do nível freático, deslocamentos, escavação, elemento finito, PLAXIS;

Abstract

In prossimità di uno scavo possono verificarsi cedimenti e danni ad infrastrutture ed edifici. Una delle cause è l'abbassamento del livello di falda necessario per eseguire lo scavo. Oggi giorno lo sviluppo di infrastrutture sotterranee richiede un'attenta analisi dell'interazione terreno-struttura al fine di preservare l'integrità delle strutture. Tale analisi assume particolare importanza quando lo scavo è eseguito in aree congestionate o quando si è in presenza di antichi edifici. Questa tesi, sviluppata presso l'Istituto Superior Técnico, presenta il caso dell'edificio Pombalino nel centro storico di Lisbona in cui negli ultimi anni è cresciuta la costruzione di infrastrutture sotterranee. Il Pombalino, risalente alla seconda metà del '700 rappresenta il simbolo della ricostruzione della città dopo il sisma del 1755 e si contraddistingue per la presenza della gabbia pombalina, una struttura lignea all'epoca installata per resistere all'azione sismica, ma oggi divenuta un elemento di debolezza della muratura. Il lavoro di tesi intende analizzare l'interazione tra il terreno e l'edificio Pombalino quando nelle vicinanze viene eseguita una riduzione del livello di falda. L'analisi è condotta con il codice agli elementi finiti PLAXIS 2D e si concentra sulla valutazione degli spostamenti al di sotto del Pombalino e sulle deformazioni indotte nella facciata dell'edificio. La gabbia pombalina è simulata attraverso il modello numerico Joint Masonry Model il quale permette di simulare le direzioni di debolezza definite dalle travi in legno e consente di stimare l'entità delle deformazioni.

Keywords

Abbassamento falda, cedimenti, scavo, elementi finiti, PLAXIS 2D;

Contents

1	Introduction	1
1.1	General overview	3
1.2	Goal	3
1.3	Thesis organization	3
2	Lisbon downtown	5
2.1	Geological and geotechnical characterization of Lisbon downtown	7
2.2	Pombalino building	12
2.3	Lisbon downtown settlements	14
3	Numerical simulation	21
3.1	Finite element method (FEM)	23
3.2	Constitutive models	23
3.2.1	Hardening Soil model and Hardening Soil model with small-strain stiffness (HSsmall)	24
3.2.1.A	HSsmall simulation	28
3.2.2	Jointed Rock Model and Masonry Model	31
3.2.2.A	Masonry model simulation	37
3.3	Drainage conditions simulated in PLAXIS 2D	41
3.3.1	Drained and undrained analysis	42
3.4	2D Model	43
3.4.1	Ground model	43
3.4.1.A	Geometry	43
3.4.1.B	Properties	44
3.4.1.C	Results	45
3.4.2	2D with underground structure	47
3.4.2.A	Geometry	47
3.4.2.B	Properties	47
3.4.2.C	Results	48

4 Case study	55
4.1 Modeling Pombalino facade	57
4.1.1 Geometry of Pombalino facade	57
4.1.2 Properties of Pombalino facade	58
4.1.3 Soil profile	59
4.1.4 Soil properties	61
4.2 Drawdown of water level	61
4.3 Results	63
5 Conclusion	73

List of Figures

2.1	Left: surface geology of the Baixa area. Right: digital terrain model (DTM) obtained from a 1:1000 survey scale. Dashed black lines separate the three defined zones (north, central and south) [1].	8
2.2	Left: thickness of anthropogenic deposits (left) and alluvial deposits (right) in Baixa [1].	9
2.3	Distribution of NSPT values in the alluvial deposits for the three zones for different depths (left) and with depth clayey and sandy materials (right) [1].	11
2.4	Example of a Pombalino building [3].	12
2.5	Foundations and frontals in a Pombalino building [4].	13
2.6	Example of wood piles in Pombalino building (left) longitudinal section and cross section (right).	13
2.7	Example of frontals in a Pombalino building (ovoodocorvo.blogspot.com).	14
2.8	Location of piezometers (blu), marks (pink) and leveling slabs (green) installed in Lisbon downtown from March 2004 to December 2010 [8].	15
2.9	Variation of water table in the alluvium layer from March 2004 to December 2010 [7].	16
2.10	Variation of water table in the miocene layer from March 2004 to December 2010 [7].	17
2.11	Map of underground constructions in Lisbon downtown [7].	18
2.12	Contour of vertical displacements measured from 2004 to 2010 in Lisbon downtown [8].	19
2.13	Behavior of surface marks, leveling slabs and measuring points recorded in Lisbon downtown [8].	20
3.1	Hyperbolic stress-strain relation in primary loading for a standard drained triaxial test [12].	25
3.2	Results from theHardin-Drnevich relationship compared to test data by Santos & Correia (2001) [12].	27
3.3	Rigidity modulus E_0 , E_{ur} and E_{50} in a triaxial test for HS_{small} model [12].	27
3.4	Triaxial test for alluvium layer: q versus ε_1 and ε_v versus ε_1	29
3.5	Triaxial test for alluvium layer: ε_v versus ε_1	29
3.6	Triaxial test for alluvium layer: τ versus σ'	30

3.7	Stiffness degradation curve.	30
3.8	Idea behind Joint Rock model [12].	31
3.9	Global and local coordinate systems in 2D conditions for the joints [10].	32
3.10	Definition of α_1 and α_2 [12].	32
3.11	Example of failure directions for JR model in PLAXIS 2D [12].	33
3.12	Definition of Plane 1 and Plane 2 in the <i>Modified Jointed Rock Model</i> [10].	34
3.13	Stress state on a portion of the masonry wall (left) and in the single brick (right) [10].	34
3.14	Geometry of panels tested. Dimensions are given in meters.	37
3.15	Total principal strain ε_1 for set a.	39
3.16	Total principal strain ε_3 for set a.	39
3.17	Total principal strain ε_1 for set b.	39
3.18	Total principal strain ε_3 for set b.	40
3.19	Total principal strain ε_1 for set c.	40
3.20	Total principal strain ε_3 for set c.	40
3.21	Geometry of the model without underground structure.	44
3.22	Principal vertical effective stress (blue) and principal horizontal effective stress (orange) at the end of water drawdown.	46
3.23	Shadings (right) and contour lines (left) of total displacement at the end of calculation.	46
3.24	Geometry of the model with underground structure.	47
3.25	Evolution of water drawdown surrounding the parking area.	49
3.26	Evolution of total displacements surrounding the parking area.	49
3.27	Evolution of vertical displacements surrounding the parking area.	50
3.28	Evolution of horizontal displacements surrounding the parking area.	50
3.29	Deformed mesh at the end of calculation.	51
3.30	Contour lines of total displacements at the end of water drawdown.	51
3.31	Arrows of total displacements at the end of water drawdown.	52
3.32	Water pressure at the end of calculation.	52
3.33	Evolution of total displacements.	53
4.1	Geometry of the real Pombalino building studied (left), and building simulated in PLAXIS 2D (right).	57
4.2	Example of Pombalino wall with frontals.	58
4.3	Geometry of the case study.	60
4.4	The generated mesh for the case study.	60
4.5	Contour lines of total displacements after the Pombalino and parking area activation (left) and at the end of water level drawdown (right).	63

4.6	Arrows of total displacements after the Pombalino and parking area activation (left) and at the end of water level drawdown (right).	63
4.7	Evolution of total displacements in the entire domain.	64
4.8	Evolution of total displacements induced only by water drawdown under Pombalino building.	65
4.9	Evolution of total displacements under Pombalino building.	66
4.10	Evolution of water drawdown under Pombalino building.	67
4.11	Evolution of total displacements under Pombalino building.	67
4.12	Evolution of vertical displacements under Pombalino building.	68
4.13	Evolution of horizontal displacements under Pombalino building.	68
4.14	Evolution of total strain ε_1 (left) and ε_3 (right) of Pombalino building ground floor at the end of water drawdown.	69
4.15	Evolution of total strain ε_1 (left) and ε_3 (right) of Pombalino building upper floors at the end of water drawdown.	69
4.16	Evolution of total strain ε_1 (left) and ε_3 (right) of Pombalino building openings at the end of water drawdown.	70
4.17	The generated deformed mesh for the case study.	70
4.18	Geometry considered to calculate distortion β	71
4.19	Intensity of damage as a function of distortion β and soil extension deformation ε_h (modified by Boscarding & Cording 1989) [13].	72
4.20	From left to right: total strain ε_1 , total strain ε_3 and deformed mesh of Pombalino building in relation to total displacements at the end of water drawdowns.	72

List of Tables

3.1	Parameters for the Hardening Soil model.	26
3.2	Parameters of the Hardening Soil with small-strain stiffness model used in the triaxial test.	28
3.3	Parameters of the Jointed Rock model.	33
3.4	Parameters of the Masonry Jointed Model.	36
3.5	Parameters of the Masonry Jointed Model for the tests.	38
3.6	Soil layers in Restauradores square.	43
3.7	Parameters of <i>ZG1</i> with Mohr Coulomb model.	44
3.8	Parameters of <i>ZG2</i> and <i>ZG3</i> with Hardening Soil with small-strain stiffness model.	45
3.9	Material properties of the diaphragm wall.	48
4.1	Parameters of Pombalino building foundations and ground floor.	59
4.2	Parameters of Pombalino building upper floors.	59
4.3	Parameters of <i>ZG2</i> and <i>ZG3</i> with Hardening Soil with small-strain stiffness model.	62
4.4	Damage categories associated with the achievement of extension limit deformation in the structure (modified by Boscarding & Cording 1989) [13].	72

Acronyms and symbols

FEM	Finite Element Method
IST	Instituto Superior Técnico
JRM	Jointed Rock Model
MM	Masonry Model
MC	Mohr-Coulomb criterium
HS	Hardening Soil Model
HSsmall	Hardening Soil with small-strain stiffness model
SPT	Standard Penetration Test

A Cross section

c Cohesion

d Thickness

e Void ratio

E Young's modulus

E_{oed} Oedometer modulus

G Shear modulus

I Moment of inertia

K Bulk modulus

K₀ Coefficient of lateral earth pressure

m Power in stress-dependent stiffness relation

n Porosity

OCR Over-consolidation ratio

p Isotropic stress or mean stress

POP Pre overburden pressure

q Deviatoric stress

u Total displacements

u_x Horizontal displacements

u_y Vertical displacements

γ Unit weight

γ Shear strain

Δ Increment

$\underline{\epsilon}$ Vector with cartesian strain components

ϵ_q Deviatoric strain

ϵ_v Volumetric strain

ν Poisson's ratio

φ Friction angle

ξ Dilatancy angle

1

Introduction

Contents

1.1 General overview	3
1.2 Goal	3
1.3 Thesis organization	3

In this chapter a general description of the subject involved in the thesis, its aim and its organization are summed up.

1.1 General overview

When an excavation is carried out, damages may be induced to buildings and infrastructures in the surrounding area. This effect gains more relevance when the soil excavated is close to cities centers or congested areas. Surface movements of the soil can generate cracks on building facade, especially in case of old buildings with historical and artistic value.

After the earthquake of 1755, downtown of Lisbon was reconstructed with the application of the first modern seismic resistant system. Structural elements strongly resistant to horizontal motions were used to build the well known Pombalino building. It has a regular and simple shape which gained historical and cultural value year after year. It has become the symbol of the reconstruction of Lisbon.

Investigations show that over the years ground settlements and fractures in Pombalino buildings have occurred. It is likely that the construction of underground infrastructures such as metro stations and parking areas might have contributed. In these situations the overburden removal generates stress relief. Moreover these types of work may require the pumping of ground water and consequently the variation of the soil stress state can produce subsidence in the ground.

This work studies a building in Lisbon downtown, with attention focused on a generic Pombalino building located in the proximity of Restauradores Square. The soil structure interaction is studied with a 2D finite element software and results are compared with total displacements measured from 2004 to 2010 by the Municipality of Lisbon.

1.2 Goal

The main goal of this dissertation is to investigate displacements under a Pombalino building when in the proximity an excavation is carried out and the water table is subjected to a sequence of drawdowns. The behaviour of the building is simulated through a numerical model which allows to characterize the response of masonry expose to the displacement field induced by the water level decrease. In other words the objective is to investigate the impact of water table drawdown and facade's damages.

1.3 Thesis organization

This document is divided in five chapters. In the first one is presented a general overview. In chapter two the geotechnical and geological characterization of Lisbon downtown is presented. Further the

main features of Pombalino building and a case history are presented. Chapter three is about the finite element theory and the numerical models used in the simulation. In order to characterize the response of the model some tests have been carried out and their results are presented. Next in chapter four the simulation of the case study is illustrated in detail. Results are shown and commented. In the end final conclusions and future developments are reported.

2

Lisbon downtown

Contents

2.1 Geological and geotechnical characterization of Lisbon downtown	7
2.2 Pombalino building	12
2.3 Lisbon downtown settlements	14

This chapter contains the results of the geological and geotechnical characterization related to the area of this work. After the description of the main features of Pombalino building a brief summary of measurements carried in Lisbon downtown is presented.

2.1 Geological and geotechnical characterization of Lisbon downtown

During its history, Lisbon has been affected by several medium to strong earthquakes that caused considerable damage and produced large economic and social impacts. In particular, the very large and well known November 1st, 1755, earthquake ($M \geq 8$) caused the complete destruction of its downtown area (Baixa), which was reconstructed with the application of the first implemented seismic resistant system [1]. Eurocode 8 presents the classification of soil into a small number of classes according to the value of the average shear-wave velocity in the upper 30 m of the surface ($v_{s,30}$). A geotechnical characterization of Lisbon downtown was performed based on the analysis of Standard Penetration Test (SPT) data compiled in the geological and geotechnical database. This database, allows the definition of 2D geological profiles used for estimating the thickness of the shallower layers. The shear-wave velocities for each layer were estimated from empirical correlations using mean SPT values computed from the statistical evaluation of the compiled data. Baixa, the downtown of Lisbon, has been occupied since prehistorical times because its strategic geographical location. After the earthquake of 1755 the most damaged area was Baixa, not only due to the site response to the strong ground motion but also due to the tsunami that followed and the fire triggered by the earthquake. Marquês de Pombal led the planning and reconstruction of Lisbon downtown, with the help of engineers and architects Manuel da Maria, Eugénio dos Santos and Carlos Mardel [2]. The new town was built over the ruins and, as a consequence of the great volume of debris, a thick layer of man-made (anthropogenic) materials, locally buried in the soft alluvial deposits, covered the creek area. Due to this process, the local coastline was artificially moved closer to its present-day location [1].

The Baixa area, located in the northern estuarine margin of the Tagus River, corresponds to the fluvial outlet of a 6,2 km² elongated basin cut in the Miocene bedrock. The valley is filled by a thick layer of alluvial sediments (normally consolidated silty sands and organic silty clays) and it is surrounded by three gentle hills [1]. The main lithologies of Baixa are showed in figure 2.1. They consist of:

- silty clayey soils and calcarenites (MPr and MFT);
- fine micaceous sandy and silty sandy soils (MEs, MQB and Mpm);
- limestones, calcarenites and coquinites (MEC, MCV and MMu);

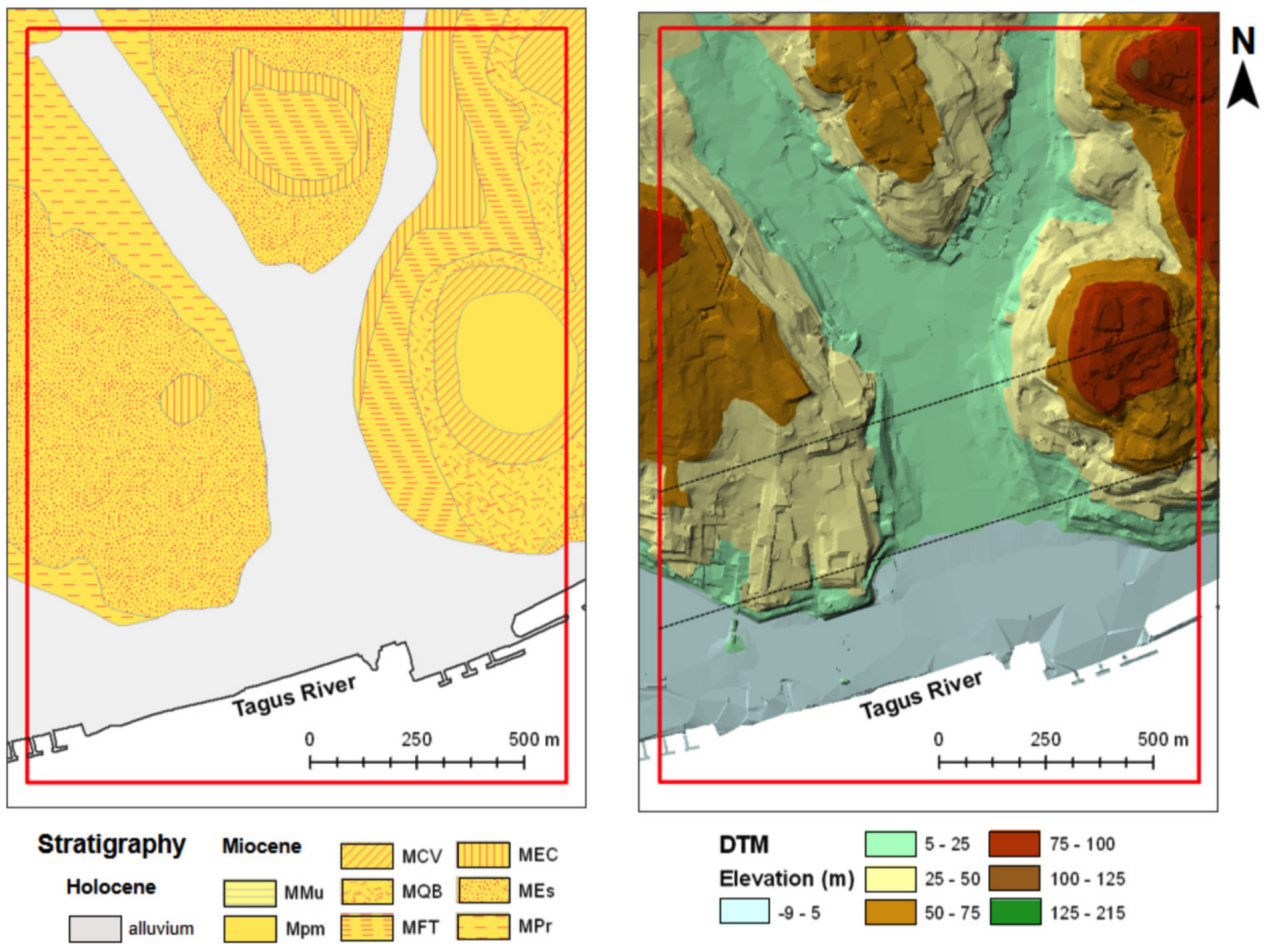


Figure 2.1: Left: surface geology of the Baixa area. Right: digital terrain model (DTM) obtained from a 1:1000 survey scale. Dashed black lines separate the three defined zones (north, central and south) [1].

As part of the *GeoSIS.Lx* research project, a geological and geotechnical database has been developed to include in situ investigation data (borehole interpretation, sampling and geotechnical measurements) and laboratory test results [1]. Based on the interpretation of the geological map and the retrieval of database information, the geological model was set. The registered data points were interpolated for the whole downtown Lisbon area, through a kriging algorithm, to determine the surfaces representing the lower boundary of each formation of interest [1]. Figure 2.2 shows anthropogenic deposits (left) and alluvial deposits (right) in Baixa.

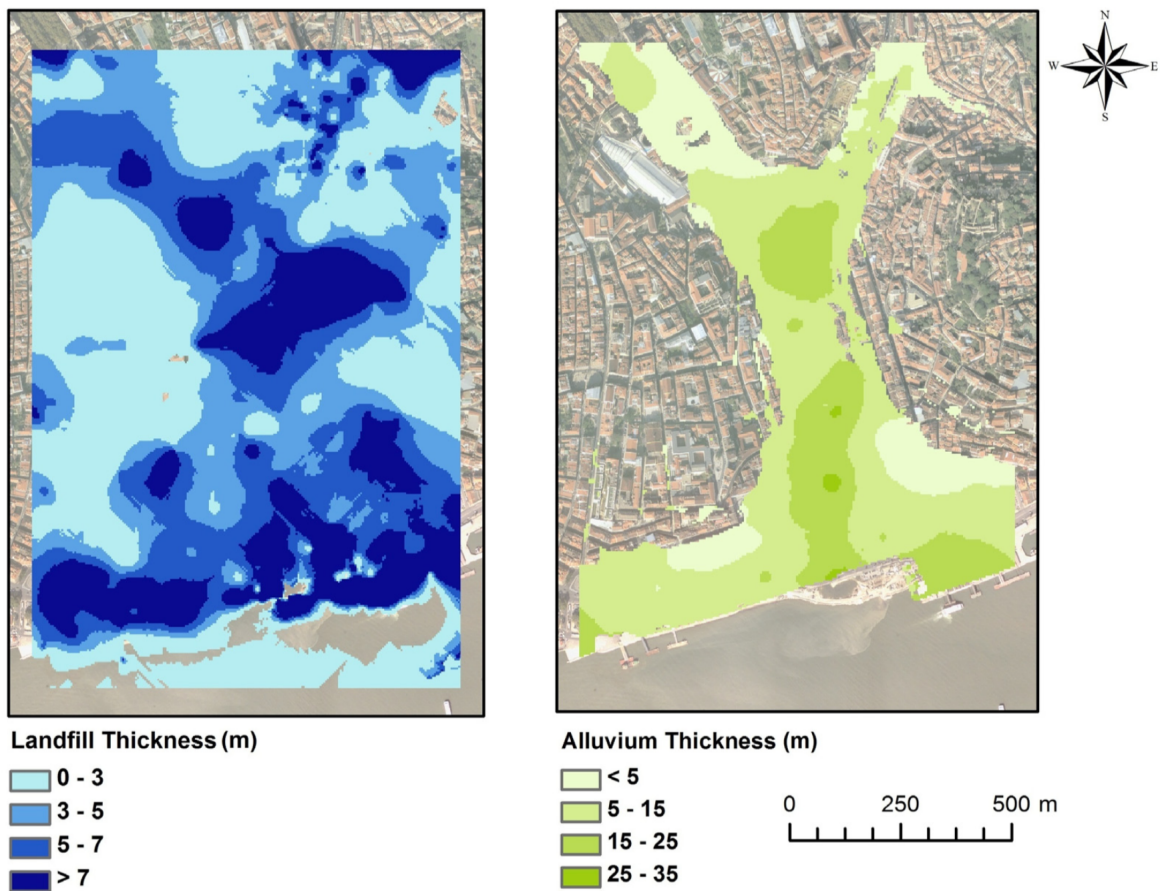


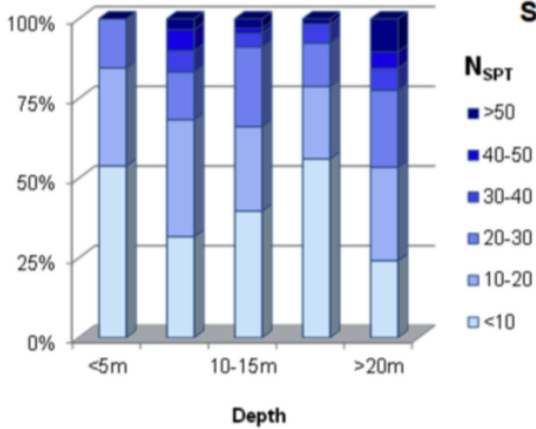
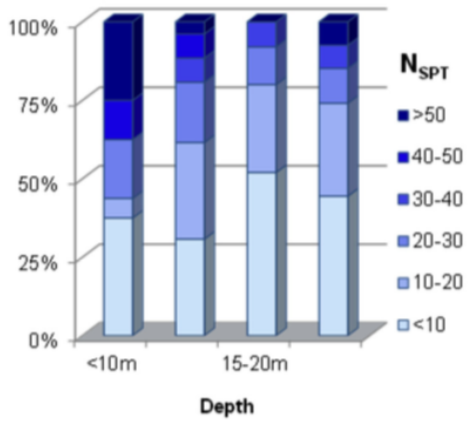
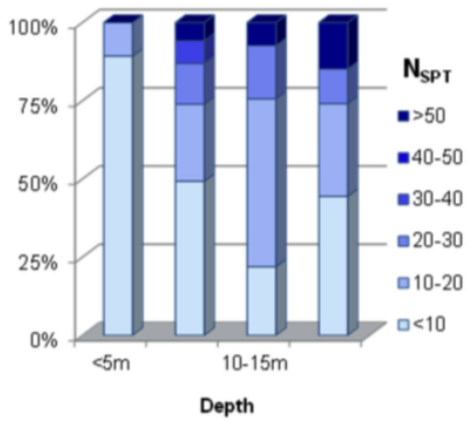
Figure 2.2: Left: thickness of anthropogenic deposits (left) and alluvial deposits (right) in Baixa [1].

Results of Standard Penetration Test (SPT) tests and lithology has been studied to perform the geotechnical characterization. The irregular spatial distribution was one of the main difficulties of the analysis. A total of 376 boreholes were selected for analysis in the Baixa area, which included 1398 N_{SPT} data values. In order to check the spatial variations of geotechnical properties due to the geological genesis and evolution of alluvial sedimentation, the area investigated was divided in three different zones (northern, central and southern) as showed in figure 2.1.

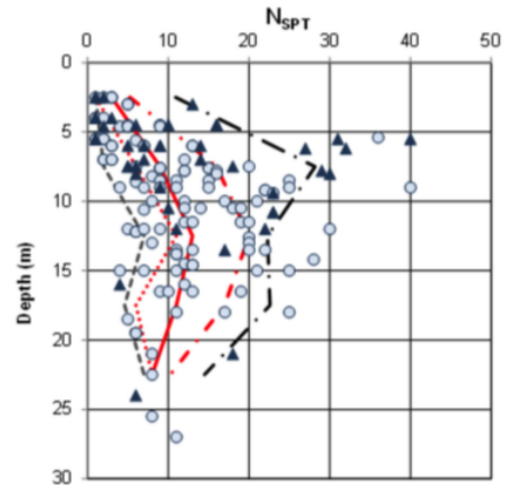
The alluvial deposits are characterized by the presence of lenticular bodies and significant lateral and vertical facies variations. The main lithological facies include soft to stiff silt and clay, loose to dense sands, and a range of transitional lithologies. The N_{SPT} values indicate the presence of normally and slightly overconsolidated soils [1]. N_{SPT} presents a remarkable irregularity. According to the authors it can be interpreted as a result of the vertical and lateral lithological variation within the lenticular bodies. Figure 2.3 shows the distribution of N_{SPT} with depth (right) and values of N_{SPT} at different depth (left) for the alluvium deposits in the three zones analyzed.

The anthropogenic deposits, which consist even on debris from the 1755 earthquake, present a heterogeneous composition. The relative distribution of N_{SPT} slightly increases with depth, due to the increasing overburden pressure.

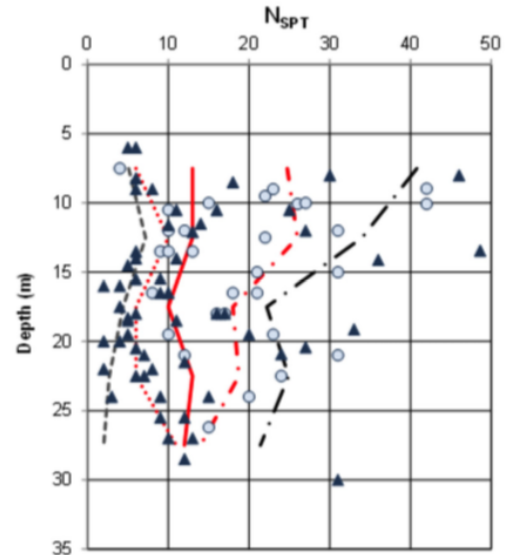
The Miocene bedrock is characterized by a sequence of sands, clays, marls, calcarenites, coquinites and limestones, with important vertical and lateral facies variations. The N_{SPT} values indicate the presence of overconsolidated stiff soils and soft rocks. The large range of values is a consequence of the heterogeneity in lithology and of the superficial degradation of the mechanical properties of the overconsolidated Miocene materials [1].



Northern



Central



Southern

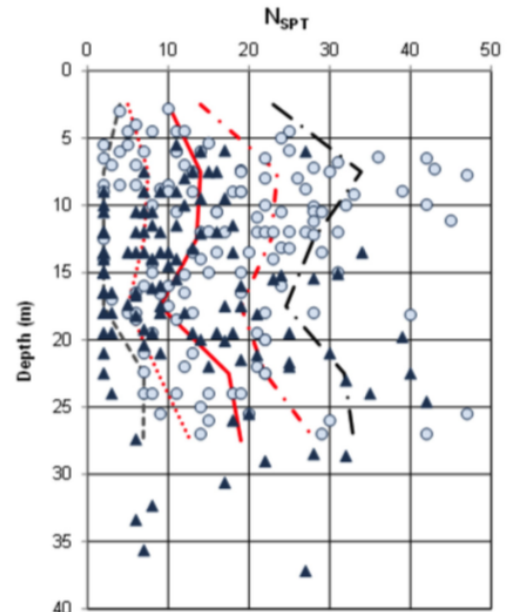


Figure 2.3: Distribution of NSPT values in the alluvial deposits for the three zones for different depths (left) and with depth clayey and sandy materials (right) [1].

2.2 Pombalino building

After the 1775 earthquake engineers and architects Manuel da Maria, Eugénio dos Santos and Carlos Mardel started to plan the construction of the new downtown of Lisbon. They decided to demolish the ruins and then to use structural elements with a relevant resistance to horizontal actions. The results were buildings with a regular and simple shape commonly called Pombalino (Figure 2.4).

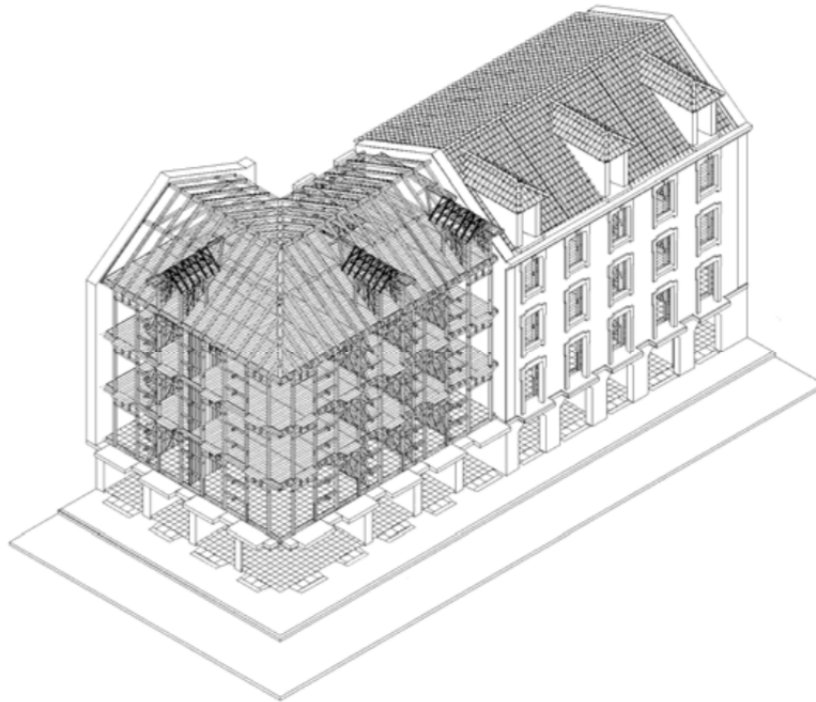


Figure 2.4: Example of a Pombalino building [3].

The downtown of Lisbon is composed of approximately sixty blocks consisting in average of seven buildings. Within each block, the buildings are constructed side by side, sharing the same gable walls. [3]. Pombalino is usually founded in short wood piles connected by arches where they settled the masonry (figure 2.6).

The ground floor was built in stone masonry in order to prevent the spread of fires and moisture coming from the ground. This type of construction confers great rigidity to the base of the building [5].

What characterized Pombalino building is the presence of frontals in the upper floors: they are formed by modules with horizontal, vertical and diagonal elements in wood (figure 2.7). The modules are filled with ordinary masonry, in order to improve the resistance of wood elements for horizontal and vertical actions. These walls are lighter than the ones made in stone masonry and at the same time they are more flexible. Floors are made of wooden beams that generally rest on the exterior and front walls, on which they discharge [6]. The external walls are very thick and stiff: they are built of stone masonry

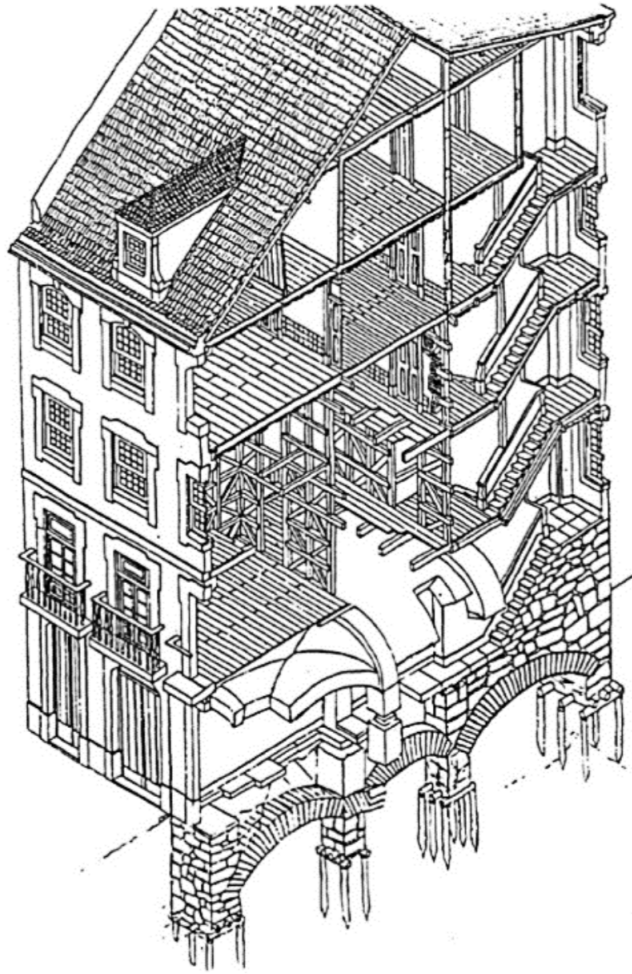


Figure 2.5: Foundations and frontals in a Pombalino building [4].

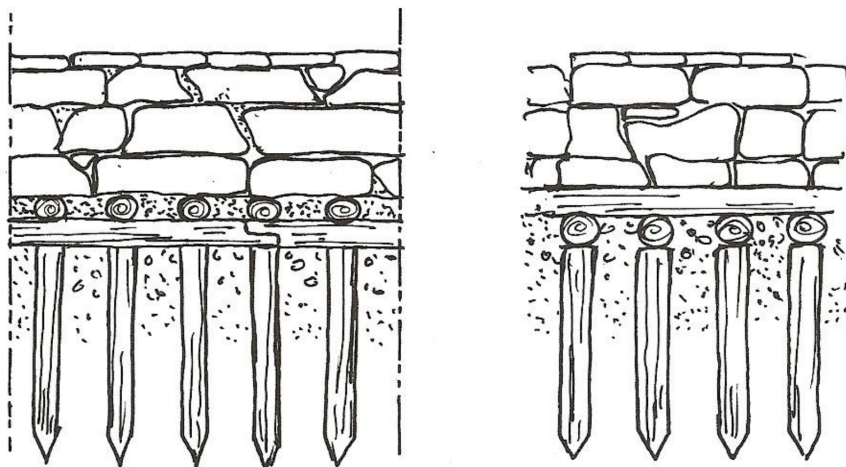


Figure 2.6: Example of wood piles in Pombalino building (left) longitudinal section and cross section (right).



Figure 2.7: Example of frontals in a Pombalino building (ovoodocorvo.blogspot.com).

joined by lime. The facade presents a large number of windows. Figure 2.5 resumes the main features of Pombalino building.

2.3 Lisbon downtown settlements

With the aim of evaluate the state of Baixa conservation, in 2003 the Municipality of Lisbon started to monitor the groundwater levels of downtown to asses their relation with ground settlements. To do that sixteen open standpipe piezometers and surface topographic marks were installed. Also leveling slabs were used to monitor vertical movements of the buildings (figure 2.8). Figures 2.9 and 2.10 show water table variations from March 2004 to December 2010 respectively in the alluvium layer and the miocene layer. The local lowering of the water table, due to the pumping for the construction of underground infrastructures, is one of the main causes of the settlements [8]. When porewater pressure decreases, the effective stress increases causing settlements.

Figure 2.11 shows the position of several underground constructions, such as car parks (from P1 to P7), lines and stations of the metro network of Lisbon. P1, in the top left corner, indicates where the parking area of Restauradores Squared is located. It corresponds to the location object of study in chapter 4. Lines in blu and green are the metro network, orange rectangles correspond to the metro station and the red line surrounds Lisbon downtown.

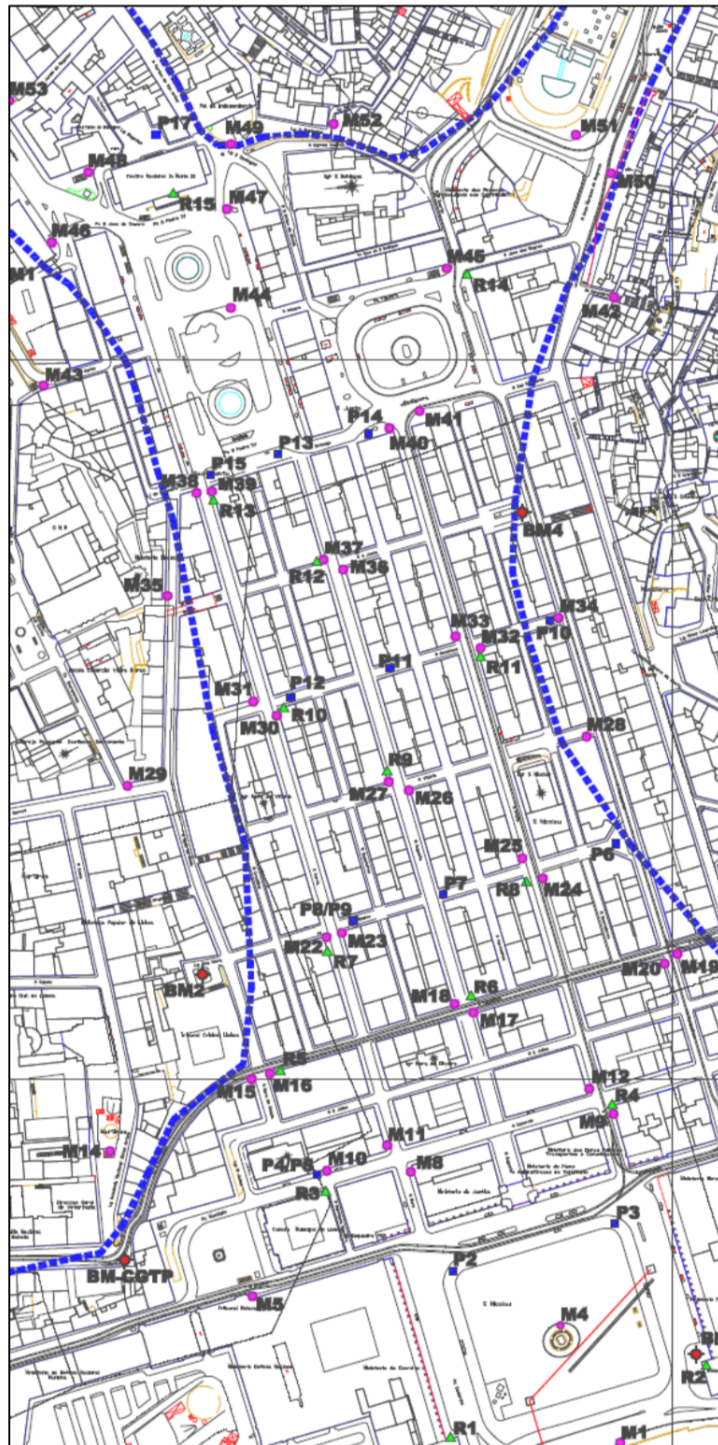


Figure 2.8: Location of piezometers (blu), marks (pink) and leveling slabs (green) installed in Lisbon downtown from March 2004 to December 2010 [8].

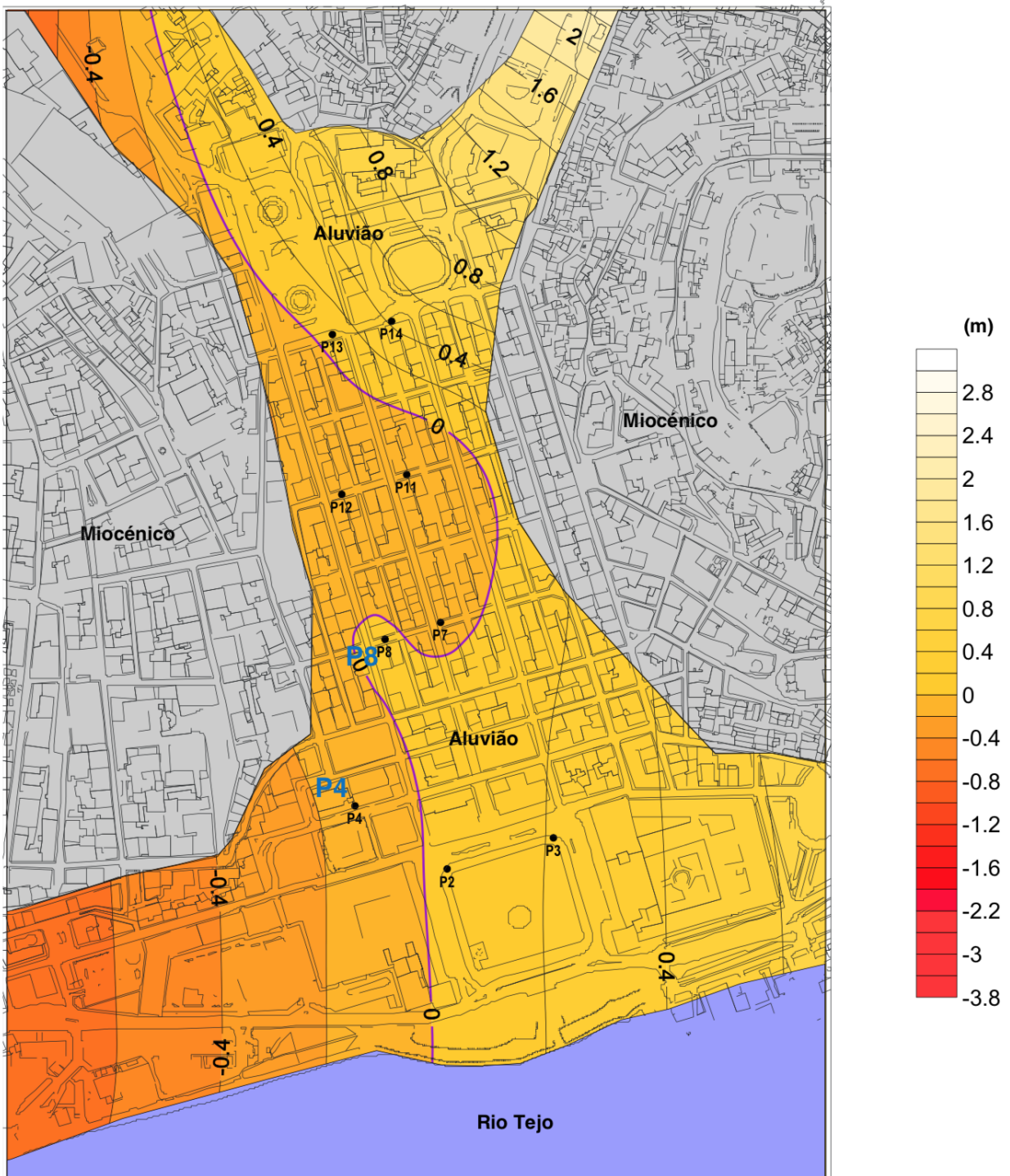


Figure 2.9: Variation of water table in the alluvium layer from March 2004 to December 2010 [7].

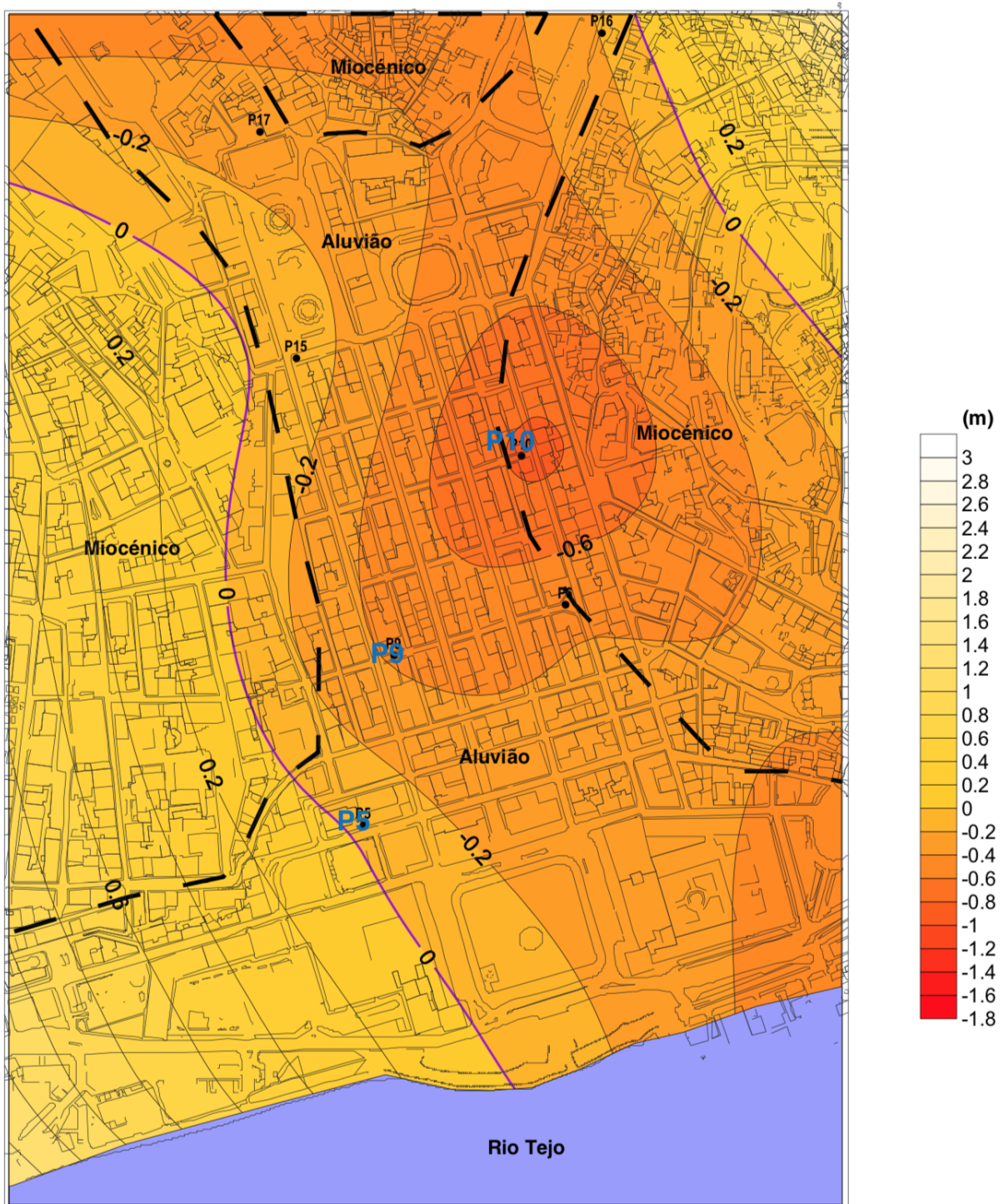


Figure 2.10: Variation of water table in the miocene layer from March 2004 to December 2010 [7].

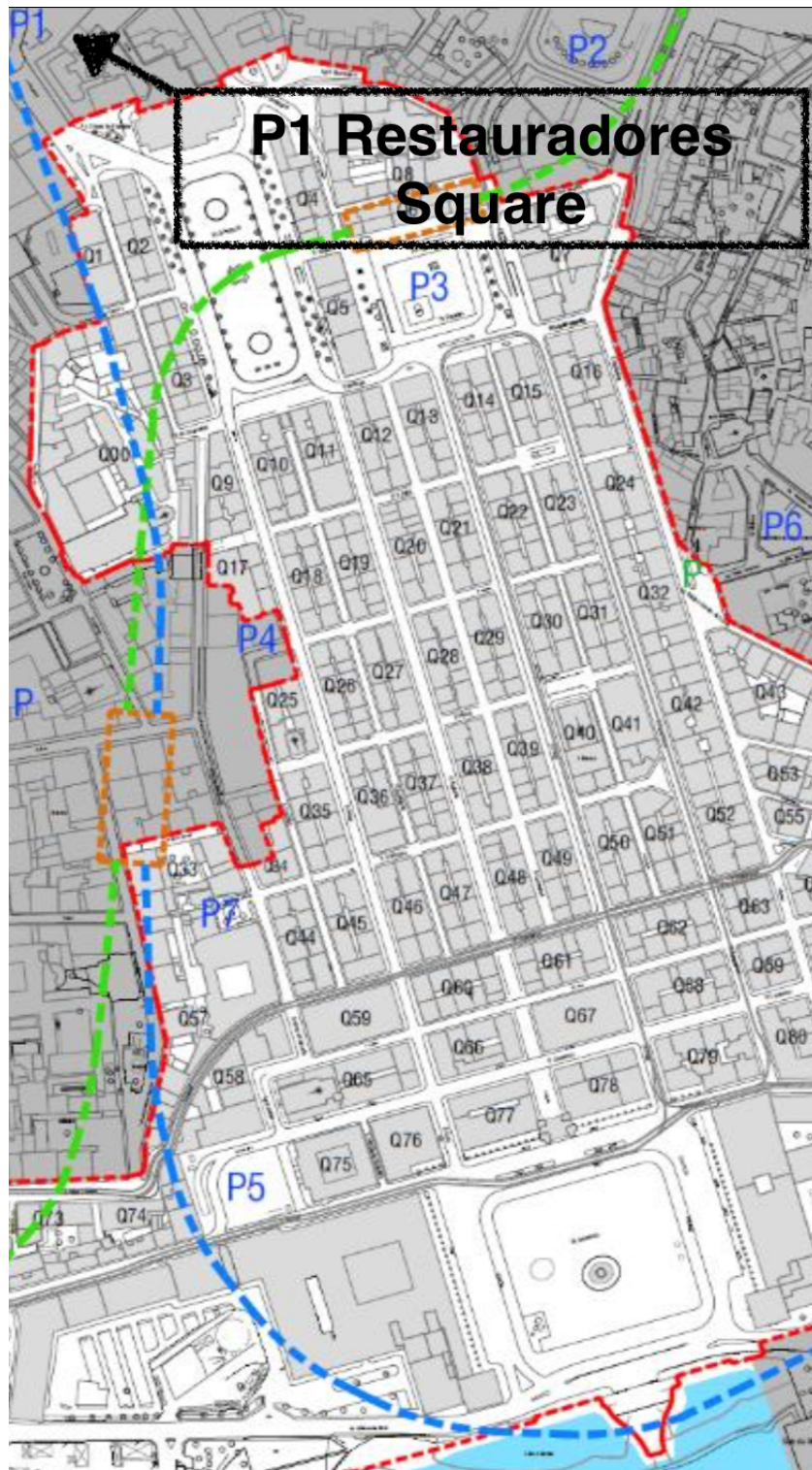


Figure 2.11: Map of underground constructions in Lisbon downtown [7].

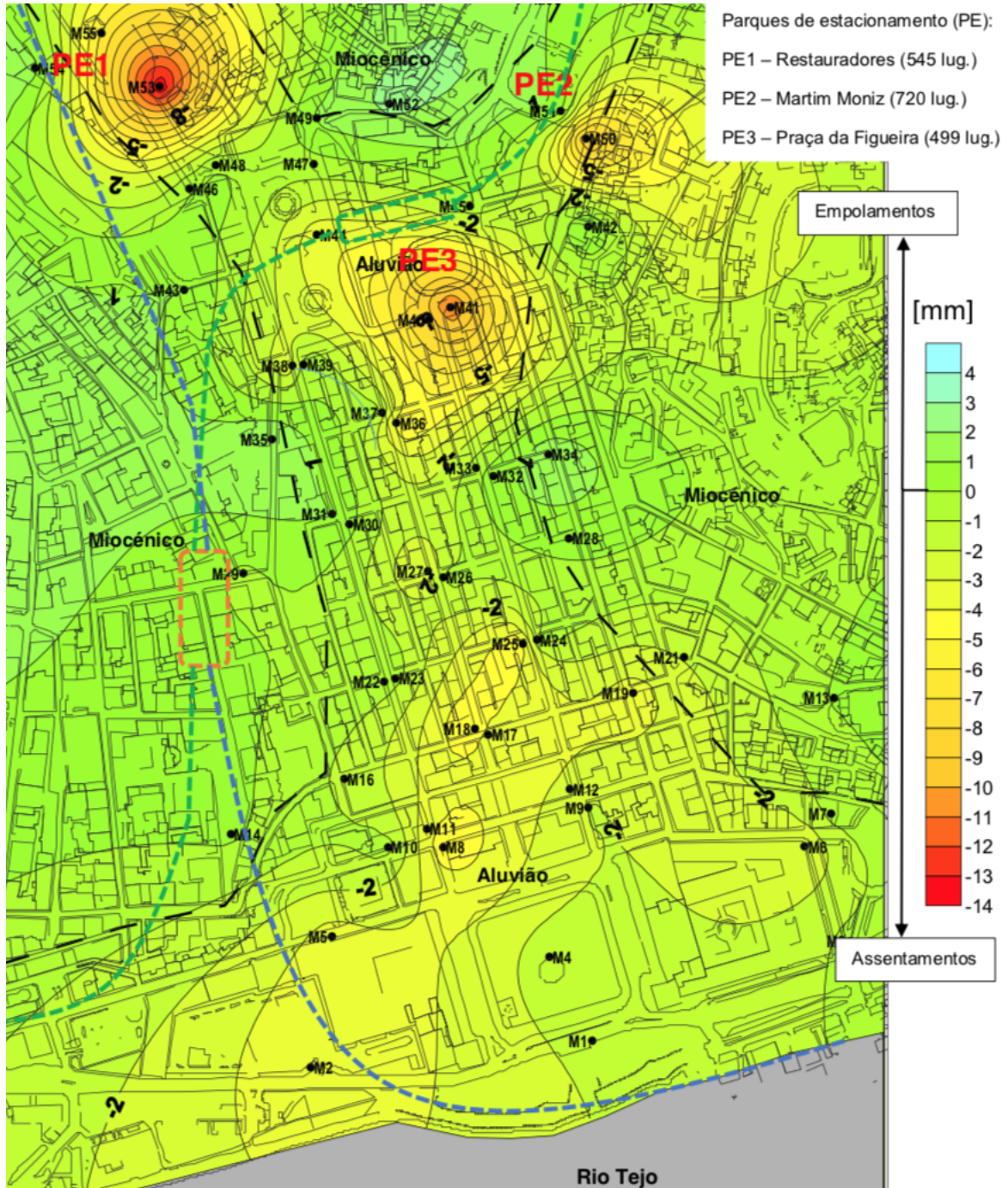


Figure 2.12: Contour of vertical displacements measured from 2004 to 2010 in Lisbon downtown [8].

The vertical displacements measured from 2004 to 2010 were used to generate the contour map shown in figure 2.12. Three areas with the same magnitude of displacements are visible, corresponding to Restauradores Square (M53 north west), Figueira Square (M41 southern than previous area) and Martim Moniz Square (M50 north east). These marks are situated close to the parking area and subway metro station, as can be seen in figure 2.11.

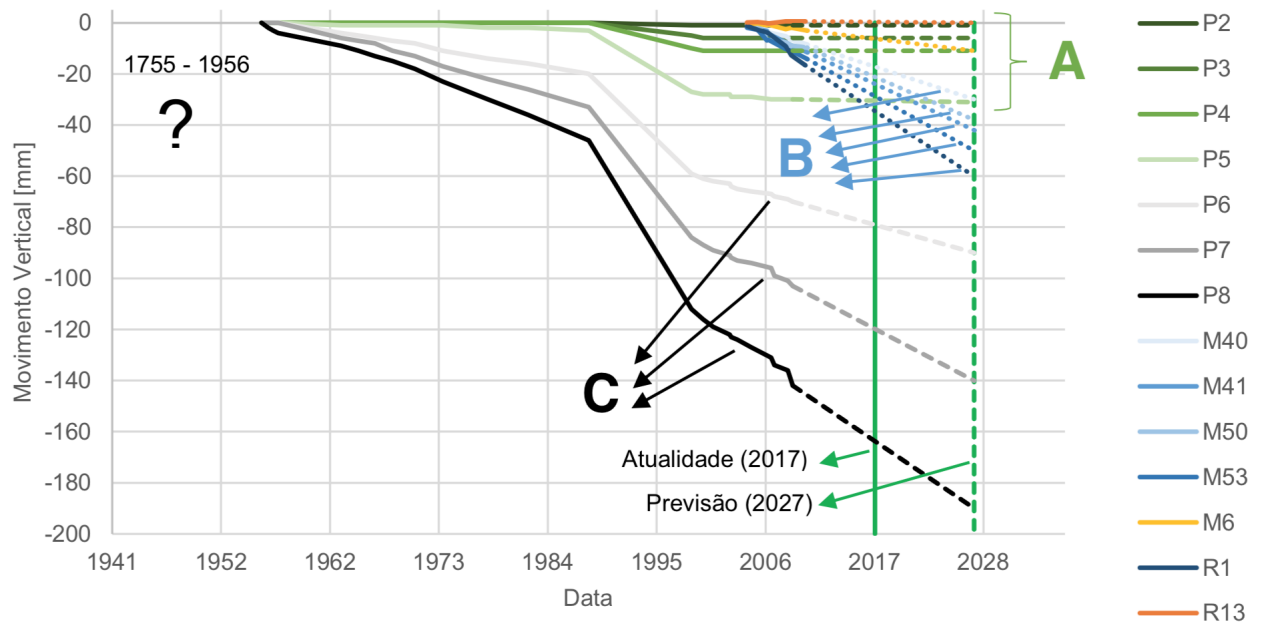


Figure 2.13: Behavior of surface marks, leveling slabs and measuring points recorded in Lisbon downtown [8].

According to Cruz [8], it is possible to distinguish three types of settlements trends of Lisbon downtown area in the period from 1956 to 2008 (figure 2.13). *Group A* represents part of the surface marks that exhibit a stabilized behavior, with no visible tendencies to increase settling. *Group B* correspond to a serie of points that show a slight tendency to increase settlements. The mark number M53 corresponding to Restauradores Squared belongs to *Group B* and shows a tendency to amplify displacements up to a value of $0,05\ m$ in 2028 [8]. Finally *Group C* has an higher rate of settlements than *Group B*. It differs from *Group B* for the rate of displacements.

3

Numerical simulation

Contents

3.1	Finite element method (FEM)	23
3.2	Constitutive models	23
3.3	Drainage conditions simulated in PLAXIS 2D	41
3.4	2D Model	43

In this chapter the finite element method (FEM) is presented. It follows a description of the main constitutive models that this work takes into account. In conclusion a 2D case with PLAXIS of a water drawdown in a soil deposit is proposed.

3.1 Finite element method (FEM)

The Finite Element Method (FEM) is a numerical method for obtaining approximate solutions to a wide variety of engineering problems. Its formulation consists on a system of algebraic equations. The method yields approximate values of the unknowns at discrete number of points over the domain. The geometry of the problem is divided in smaller parts called finite elements. The system of algebraic equations is composed by the simple equations that model each finite elements. To approximate a solution FEM minimizes an error function associated to the calculation of the unknowns.

The software that I used in this thesis for the study of the soil and building interaction is PLAXIS 2D.

The geometry of the boundary value problem under investigation should be defined and quantified. Simplifications and approximations may be necessary during this process. This geometry is then replaced by an equivalent finite element mesh which is composed of small regions called finite elements [9]. Usually the finite elements corresponds to triangular or quadrilateral in shape for two dimensional problems. Nodes are key points of the finite element because their coordinates define the geometry of the element. Each finite element is systematically numbered in order to refer to the complete finite element mesh. It is important to underline that the geometry of the boundary value problem should be approximated as accurately as possible. For that reason in the case of discontinuities, interfaces between materials with different properties and applied boundary conditions is possible to introduce new finite elements and nodes. In order to obtain accurate solutions, these zones require a refined mesh of smaller elements [9]. The situation is more complex for general nonlinear material behaviour, since the final solution may depend, for example, on the previous loading history [9]. It is necessary to define with accuracy the boundary conditions and the material properties. For these materials the loading history should be divided into a number of solution increments and a separate finite element solution obtained for each increment. The incremental global stiffness matrix is not constant but varies during the increment with stress and or strain. For that reason a solution strategy is necessary to take into account this changes in material behaviour.

3.2 Constitutive models

It is well known that soil and rock behaviour is highly non-linear and complex. This non-linear stress-strain behaviour can be modeled at several levels of sophistication. The constitutive models have a great

influence on the results obtained in the modeling. The more complex models tend to represent better the behavior of the materials, however the amount of parameters needed is higher and some don't have physical meaning. Moreover data for their correct definition are not always available. PLAXIS supports different models to simulate the behaviour of soil. Due to the complexity of the strain-strain relationship and the small strain induced in the soil, in this work the following models have been used: Hardening Soil small-strain stiffness (HSsmall), and Masonry model, a modeled version of the Jointed Rock model [10]. In the next section these models are described in detail.

3.2.1 Hardening Soil model and Hardening Soil model with small-strain stiffness (HSsmall)

To simulate the soil behaviour it is possible to use the Hardening Soil with small-strain stiffness model (HSsmall) which is an elastoplastic type of hyperbolic model, formulated in the framework of shear hardening plasticity. It involves compression hardening to represent irreversible compaction of soil under compression. Moreover it allows for a more realistic representation of soil behavior, particularly in the consideration of unload and reload cycles such as successive stages of excavation [11].

Unlike to an elastic perfectly-plastic model, the yield surface of a hardening plasticity model is not fixed in principal stress space, but it can expand due to plastic straining. Distinction can be made between two main types of hardening, namely shear hardening and compression hardening. The first one is used to model irreversible strains due to primary deviatoric loading. The second hardening is used to model irreversible plastic strains due to primary compression in oedometer loading and isotropic loading. The Hardening Soil Model (HS) considers both types of hardening.

Some basic characteristics of the model are:

- stress dependent stiffness according to a power law (parameter m);
- plastic straining due to primary deviatoric loading (parameter E_{50}^{ref});
- plastic straining due to primary compression (parameter E_{oed}^{ref});
- elastic unloading / reloading (parameters E_{ur}^{ref} , ν_{ur});
- failure according to the Mohr-Coulomb failure criterion (parameters c' , φ);

The vertical strain ε_1 and the deviatoric stress q are related by an hyperbolic relationship in primary triaxial loading. This is represented in figure 3.1. Equation 3.1 describes this behaviour for $q < q_f$:

$$-\varepsilon_1 = \frac{1}{E_i} \frac{q}{1 - q/q_a} \quad (3.1)$$

where E_i is related to E_{50} by:

$$E_i = \frac{2E_{50}}{2 - R_f} \quad (3.2)$$

The parameter E_{50} is the confining stress dependent stiffness modulus for primary loading and is provided by equation 3.3:

$$E_{50} = E_{50}^{ref} \left(\frac{c \cos \varphi - \sigma'_3 \sin \varphi}{c \cos \varphi + p^{ref} \sin \varphi} \right)^m \quad (3.3)$$

where E_{50}^{ref} is a reference stiffness modulus corresponding to the reference confining p^{ref} .

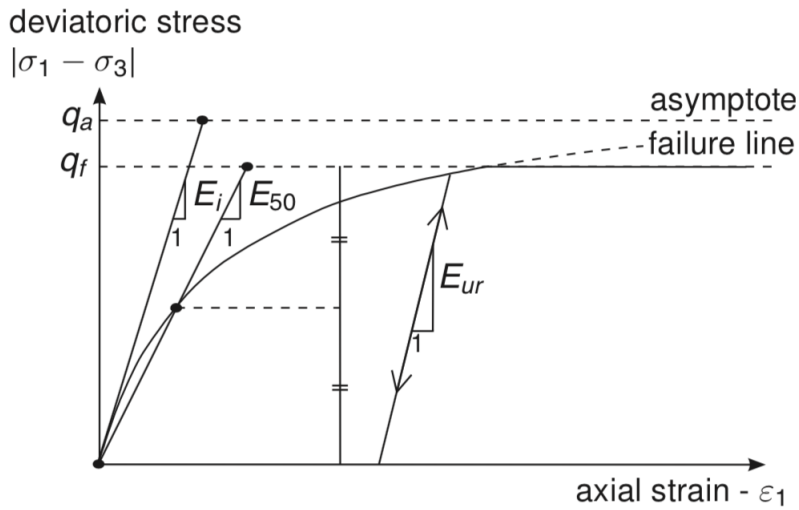


Figure 3.1: Hyperbolic stress-strain relation in primary loading for a standard drained triaxial test [12].

The parameters for the Hardening Soil model are listed in table 3.1.

To simulate small-strain stiffness two additional parameters which describe the behaviour of stiffness in the range of small deformations are needed:

- the initial or very small-strain shear modulus G_0 ;
- the shear strain level $\gamma_{0.7}$ at which the secant shear modulus G_s is reduced to about 70% of G_0 ;

Test data highlights that the stress-strain curve for small strains can be described by a simple hyperbolic law. The Hardin-Drnevich relationship (eq 3.4) describes well this phenomenon:

$$\frac{G_s}{G_0} = \frac{1}{1 + \left| \frac{\gamma}{\gamma_r} \right|} \quad (3.4)$$

where γ_r is the threshold shear strain and is given by:

$$\gamma_r = \frac{\tau_{max}}{G_0} \quad (3.5)$$

Table 3.1: Parameters for the Hardening Soil model.

Symbol	Meaning	Unit
<i>Failure parameters as in MC model</i>		
c	(Effective) cohesion	kN/m^2
φ	(Effective) angle of internal friction	$^\circ$
ψ	Angle of internal friction	$^\circ$
σ_t	Tension cut-off and tensile strength	kN/m^2
<i>Basic parameters for soil stiffness</i>		
E_{50}^{ref}	Secant stiffness in standard drained triaxial test	kN/m^2
E_{oed}^{ref}	Tangent stiffness for primary oedometer loading	kN/m^2
E_{ur}^{ref}	Unloading / reloading stiffness	kN/m^2
m	Power for stress-level dependency of stiffness	
<i>Advanced parameters</i>		
ν_{ur}	Poisson's ratio for unloading-reloading (default $\nu_{ur} = 0,2$)	
p^{ref}	Reference stress stiffnesses (default $p^{ref} = 100$)	kN/m^2
K_0^{nc}	K_0 -value for normal consolidation (default $K_0^{nc} = 1 - \sin \varphi$)	
R_f	Failure ratio q_f/q_a (default $R_f = 0,9$)	
$\sigma_{tension}$	Tensile strength (default $\sigma_{tension} = 0$)	kN/m^2

where τ_{max} is the shear stress at failure.

Equations 3.4 and 3.5 can be considered for large strains. More straightforward and less prone to error is the use of a smaller threshold shear strain. Santos & Correia (2001), for example suggest to use the shear strain $\gamma_r = \gamma_{0,7}$ at which the secant shear modulus G_s is reduced to about 70% of its initial value [12]. Equation 3.4 become:

$$\frac{G_s}{G_0} = \frac{1}{1 + a|\frac{\gamma}{\gamma_r}|} \quad (3.6)$$

If a value of a equal to 0,385 is considered, a value of $\frac{G_s}{G_0}$ equal to 0,772 is reached.

G_0 can be determined by measuring the tensions and deformations considering "small" loads or by measuring shear wave's velocity (wave propagation theory). In PLAXIS ν_{ur} is considered constant so the shear modulus G_0^{ref} is computed from the very small strain Young's modulus as:

$$G_0^{ref} = \frac{E_0^{ref}}{2(1 + \nu_{ur})} \quad (3.7)$$

Finally to determine $\gamma_{0,7}$ is possible to use Ishibashi and Zhang (1993) equation (eq 3.8):

$$\frac{G}{G_0} = K(\gamma, IP)(p')^{m(\gamma, IP) - m_0} \quad (3.8)$$

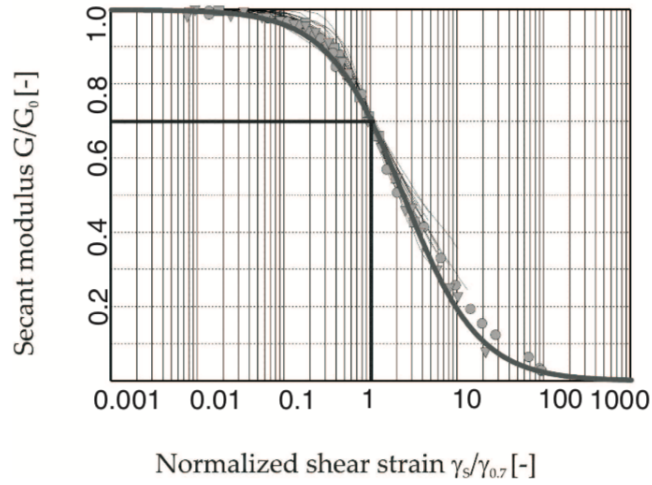


Figure 3.2: Results from the Hardin-Drnevich relationship compared to test data by Santos & Correia (2001) [12].

Where:

$$K(\gamma, IP) = 0,5 \left[1 + \tanh \left(\ln \left(\frac{0,000102 + n(IP)}{\gamma} \right)^{0,492} \right) \right] \quad (3.9)$$

$$m(\gamma, IP) - m_0 = 0,272 \left[1 - \tanh \left(\ln \left(\frac{0,000556}{\gamma} \right)^{0,4} \right) \right] \exp(-0,0145IP^{1,3}) \quad (3.10)$$

Figure 3.3 illustrates for *HSsmall* model the rigidity modulus E_0 , E_{ur} and E_{50} in a triaxial test.

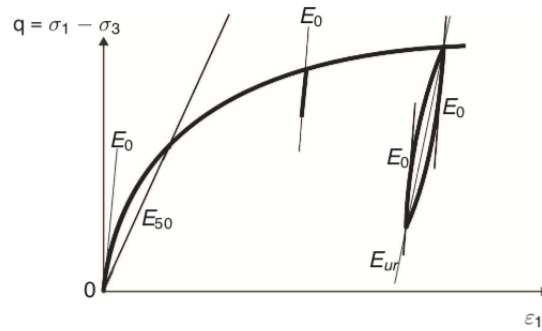


Figure 3.3: Rigidity modulus E_0 , E_{ur} and E_{50} in a triaxial test for *HSsmall* model [12].

3.2.1.A HSsmall simulation

In order to characterize the response of the numerical model a triaxial test was carried out in PLAXIS for alluvium layer. Parameters used in the test were obtained by the geological surveys of *GeoSIS.Lx* research project and they are presented in table 3.2. They are representative of the alluvium layer ZG2 considered in the case study. PLAXIS 2D function *SoilTest* enables to simulate real life soil tests such as triaxial test which lets to test soil properties while controlling the stresses applied in the vertical and horizontal directions. The vertical preconsolidation stress σ_1 and the initial effective stress σ'_3 are equal to 100 *kPa*.

Table 3.2: Parameters of the Hardening Soil with small-strain stiffness model used in the triaxial test.

Parameter	Meaning	Value	Unit
$Type$	Drainage type	<i>Drained</i>	-
γ_{unsat}	Soil unit weight above p.l.	17,6	<i>kN/m³</i>
γ_{sat}	Soil unit weight below p.l.	17,6	<i>kN/m³</i>
c'_{ref}	(Effective) cohesion	0,00	<i>kN/m²</i>
φ'	(Effective) angle of internal friction	29,00	°
ψ	Dilatancy angle	0,00	°
E_{50}^{ref}	Secant stiffness in standard drained triaxial test	125,0E3	<i>kN/m²</i>
E_{oed}^{ref}	Tangent stiffness for primary oedometer loading	125,0E3	<i>kN/m²</i>
E_{ur}^{ref}	Unloading / reloading stiffness	375,0E3	<i>kN/m²</i>
m	Power for stress-level dependency of stiffness	0,5	
$\gamma_{0.7}$	Shear strain at which $G_s = 0.722G_0$	0,3E-3	
G_0^{ref}	Shear modulus at very small strains	145,0E3	<i>kN/m²</i>
ν'_{ur}	Poisson's ratio	0,3	-

Results of the triaxial compression isotropic test (drained conditions), are showed in figures 3.4, 3.5 and 3.6. In the first one is possible to observe that the deviator stress progressively increases until large deformations of the order of 0,7% are attained. For small values of ε_1 soil behaviour can be assume elastic. Simultaneously the specimen continuously reduces its volume and only at large deformations shear strains occur without any further volume change (figure 3.5). Figure 3.6 shows the failure line according to MC criterium. Figure 3.7 shows stiffness degradation curve obtained by repeating the test with $|\varepsilon_1|$ equals to 1%, 0,1% and 0,01%.

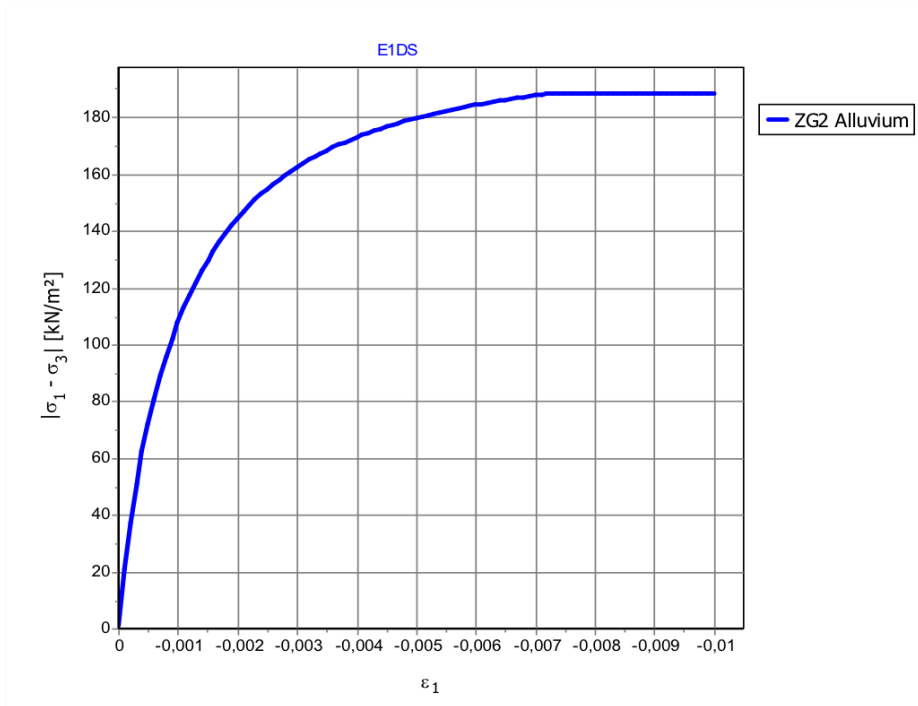


Figure 3.4: Triaxial test for alluvium layer: q versus ϵ_1 and ϵ_v versus ϵ_1 .

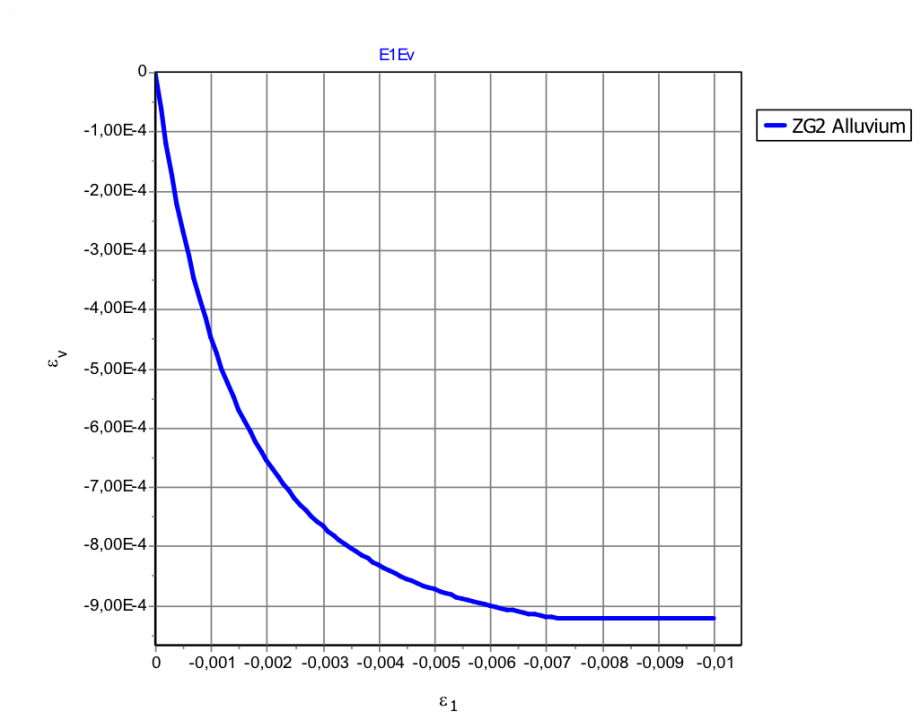


Figure 3.5: Triaxial test for alluvium layer: ϵ_v versus ϵ_1 .

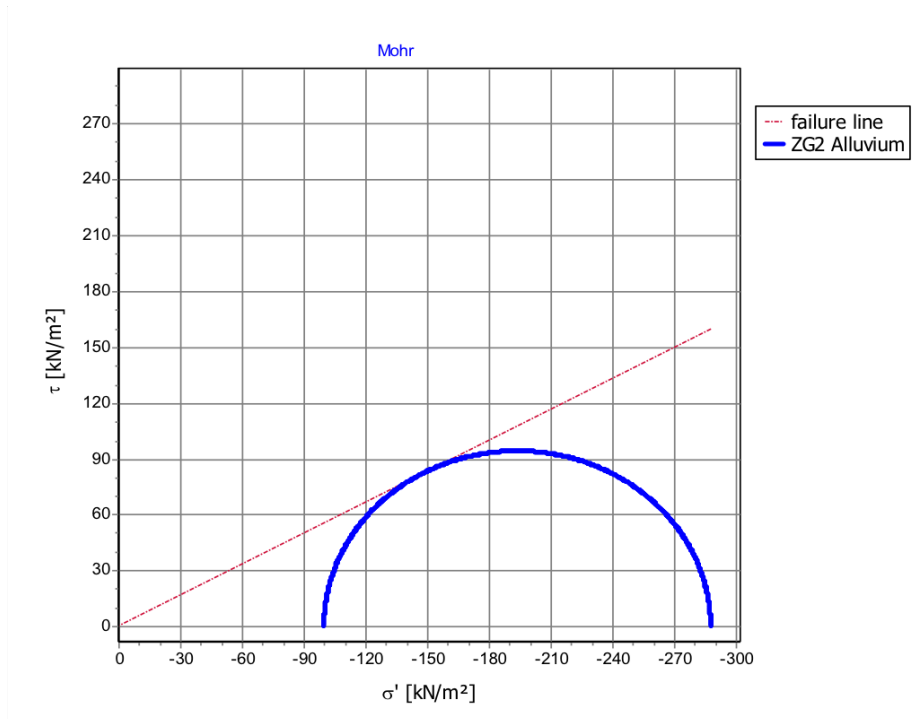


Figure 3.6: Triaxial test for alluvium layer: τ versus σ' .

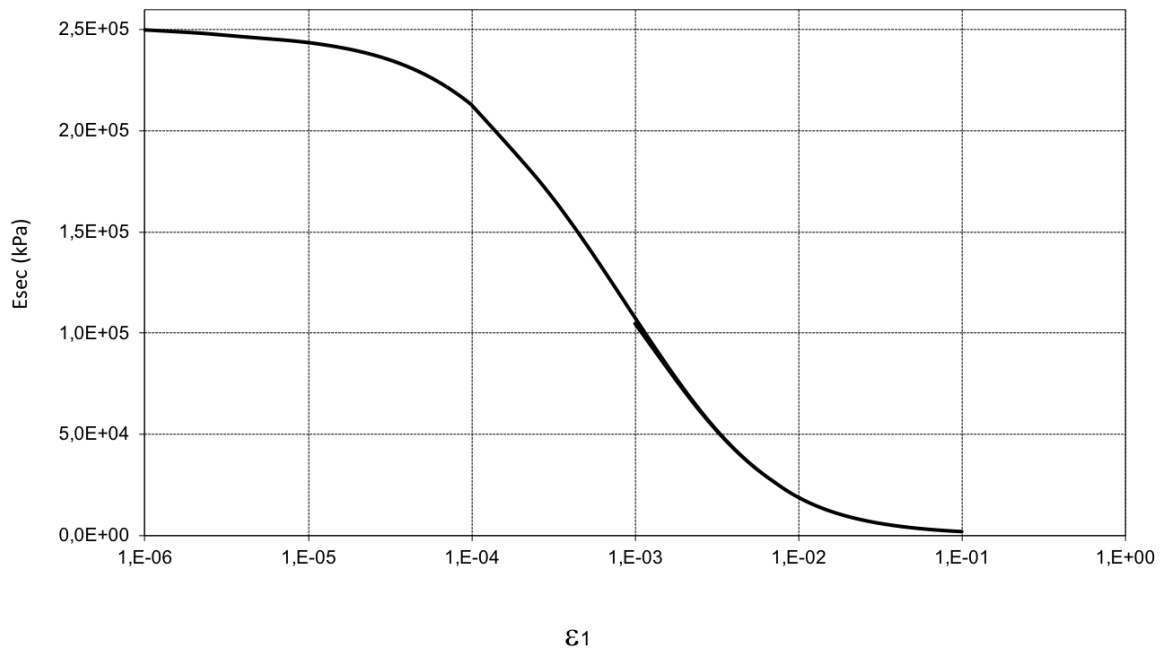


Figure 3.7: Stiffness degradation curve.

3.2.2 Jointed Rock Model and Masonry Model

Anisotropy is the property of being directionally dependent, which involves different properties in different directions. Materials characterized by anisotropy respond differently when subjected to specific conditions in one direction rather than another [12]. The Jointed Rock model Jointed Rock Model (JRM) simulates plastic anisotropy by using different strength properties in different directions.

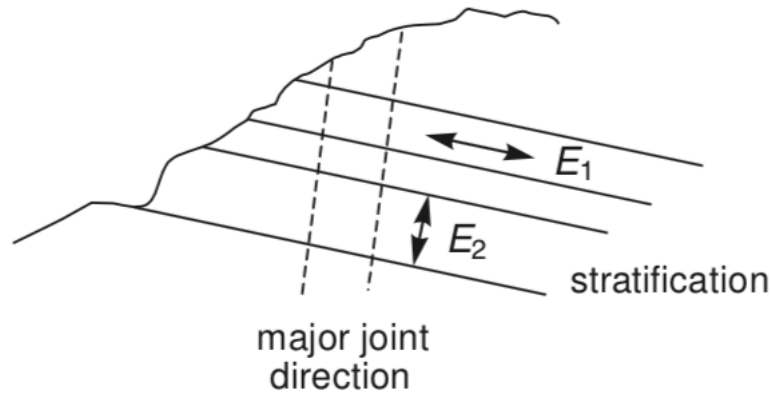


Figure 3.8: Idea behind Joint Rock model [12].

Joint Rock is an anisotropic elastic-perfectly plastic model where plastic shearing can only occur in a limited number of shearing directions. For that reason it is assumed that the rock is intact and an optional stratification direction is present [12]. The intact rock is considered as an anisotropic elastic material characterized by five parameters and a direction.

The Joint Rock Model considers in its formulation a maximum of three different rock-mass discontinuity planes along which a Mohr-Coulomb Mohr-Coulomb criterium (MC) yield criterion holds with tension cut-off. A maximum of three sliding directions can be chosen and they can have different shear strength properties. Figure 3.9 shows coordinate systems in 2D conditions for joints. The MC and tensile-cut off yield functions are defined respectively by equations 3.11 and 3.12 for $i = 1 \dots n_{p0}$:

$$f_i^c = |\tau_{s,i}| + \sigma_{n,i} \tan \varphi_i - c_{0,i} \quad (3.11)$$

$$f_i^t = \sigma_{n,i} - \sigma_{t0,i} \quad (3.12)$$

Where:

- $i = 1 \dots n_{p0}$ with $n_{p0} \leq 3$ is the specific orientation considered;
- $\sigma_{n,i}$ is the normal stress along orientation i ;

- $\tau_{n,i}$ is the shear stress along orientation i ;
- $c_{0,i}$ is the cohesion;
- φ_i is the friction angle;
- $\sigma_{t0,i}$ is the tensile strength with $\sigma_{t0,i} \leq c_{0,i} \cot \varphi_i$;

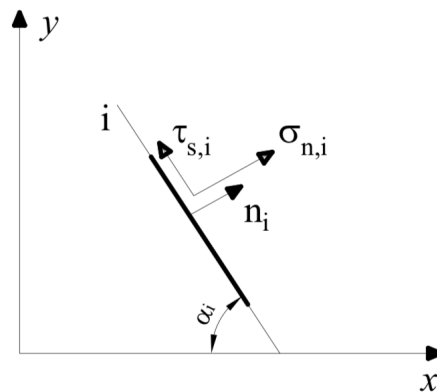


Figure 3.9: Global and local coordinate systems in 2D conditions for the joints [10].

In general the JR model is useful when families of joints are present. They have to be parallel and their spacing has to be small compared to the dimension of the entire block. Most parameters of the Jointed Rock model coincide with those of the isotropic Mohr-Coulomb model (table 3.3).

The **JR!** (**JR!**) assumes that the direction of elastic anisotropy is the first one where plastic shearing can occur ("plane 1") and has to be always specified. Two parameters describe the sliding directions: α_1 called *Dip angle* and α_2 called *Strike*. Figure 3.10 illustrates the meaning of these two parameters.

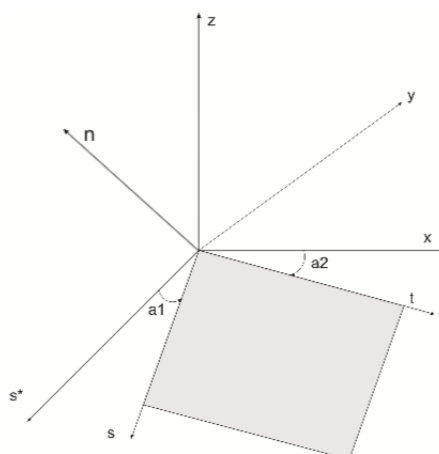


Figure 3.10: Definition of α_1 and α_2 [12].

α_1 can be defined as the positive 'downward' inclination angle between the horizontal plane and the

Table 3.3: Parameters of the Jointed Rock model.

Parameter	Meaning	Unit
<i>Elastic parameters as in MC model</i>		
E_1	Young's modulus for rock as a continuum	kN/m^2
ν_1	Poisson's ratio for rock as a continuum	-
<i>Anisotropic elastic parameters Plane 1 direction</i>		
E_2	Young's modulus perpendicular on plane 1 direction	kN/m^2
G_2	Shear modulus perpendicular on plane 1 direction	kN/m^2
ν_2	Poisson's ratio perpendicular on plane 1 direction	-
<i>Strength parameters in joint directions (plane $i = 1, 2, 3$)</i>		
c_i	Cohesion	kN/m^2
φ_i	Friction angle	°
ψ_i	Dilatancy angle	°
$\sigma_{t,i}$	Tensile strength	kPa
<i>Definition of joint directions (plane $i = 1, 2, 3$)</i>		
n	Number of joint directions ($1 \leq n \leq 3$)	-
$\alpha_{1,i}$	Dip ($-180 \leq \alpha_{1,i} \leq 180$)	°
$\alpha_{2,1}$	Strike ($-180 \leq \alpha_{1,i} \leq 180$) ($\alpha_{2,i} = 90$ in PLAXIS 2D)	°

sliding plane. α_2 is defined in PLAXIS as the orientation of the vector t respect to the x -direction [12]. Figure 3.11 shows an example of failure directions.

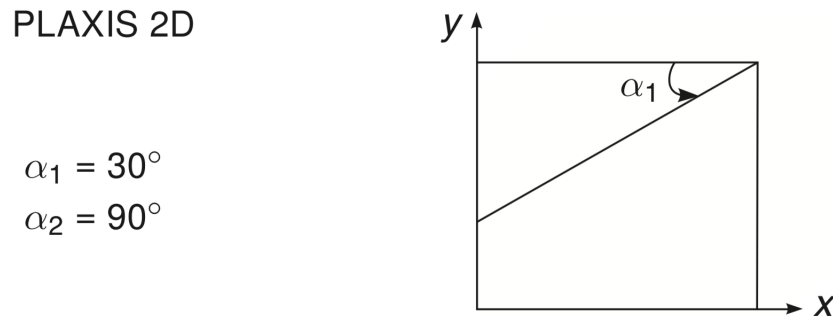


Figure 3.11: Example of failure directions for JR model in PLAXIS 2D [12].

The *Masonry Model* Masonry Model (MM) is a modified version of the *Jointed Rock Model* and it has been formulated with the aim of investigate the interaction between tunneling and historical masonry structures [10]. The idea is to schematise the block masonry structure as a homogenised anisotropic medium. Similarly to fractured rocks, ancient masonry structures are characterised by high strength units, such as stone blocks or bricks, with weak joints, either dry joints or lime mortar joints, that represent the possible discontinuities where the cracks tend to develop [10]. When failure occurs it is possible to

observe the crack pattern along the discontinuity planes represented by the joints. However in the case of masonry facade, a further strength, against the opening of vertical failure surfaces, is provided by the interlocking of masonry units. The modifies applied to the *JRM* can be discuss in relation to figure 3.12 [10] in which is possible to distinguish two families of joints: plane 1 is related to the head joints and plane 2 to the bed joints.

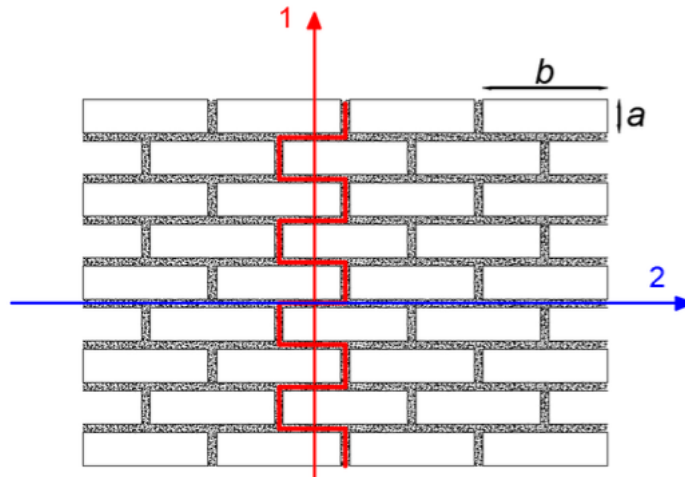


Figure 3.12: Definition of Plane 1 and Plane 2 in the *Modified Jointed Rock Model* [10].

The modification consists in taking into account for plane 1 the enhanced tensile strength available due to the contribution of the bed joints, which are subjected to a vertical stress state which increases with depth [10]. This contribution can be better understand by looking to figure 3.13. The portion of the wall is subjected to a vertical compressive stress σ_2 and to a horizontal tensile stress σ_1 . At the same time each single brick is subjected to a compressive stress $\sigma_{n,2} = \sigma_2$, a tensile stress $\sigma_{n,1} \leq \sigma_1$ and a tangential stress $\tau_{s,2}$ on the bed joints due to the friction among the blocks.

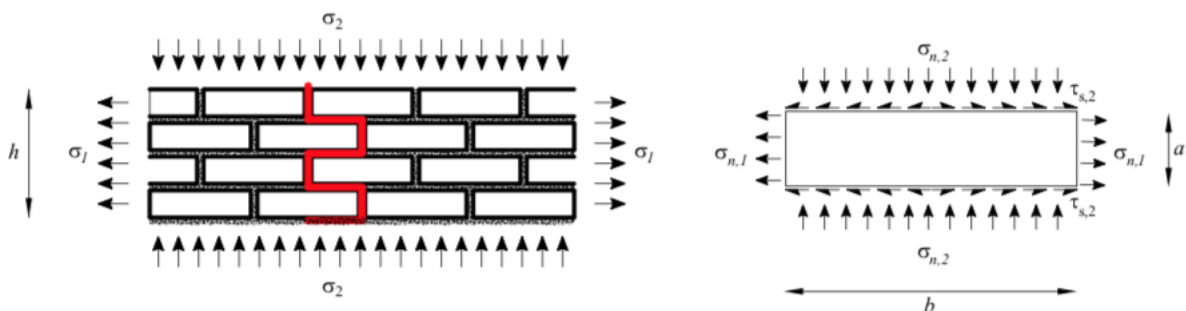


Figure 3.13: Stress state on a portion of the masonry wall (left) and in the single brick (right) [10].

Considering valid equations 3.11 and 3.12 is possible to formulate the macroscopic tensile strength $\sigma_{t,1}$ along direction 2 with equation 3.13:

$$\sigma_{t,1} = \sigma_{t0,1} + \frac{n}{h}(c_{0,2} + \sigma_{n,2} \tan \varphi_2) \frac{b}{2} \quad (3.13)$$

Where n is the number of bed joints. Equation 3.13 can be reformulated considering that $h = a \cdot n$.

$$\sigma_{t,1} = \sigma_{t0,1} + \frac{b}{2a}c_{0,2} + \frac{b}{2a}\sigma_{n,2} \tan \varphi_2 \quad (3.14)$$

Where:

- $\sigma_{t0,1}$ is the contribution of tensile strength;
- $\frac{b}{2a}c_{0,2}$ is the cohesive contribution;
- $\frac{b}{2a}\sigma_{n,2} \tan \varphi_2$ is the frictional contribution;

Without considering the interlocking of blocks as in the *Jointed Rock Model* equation 3.14 should be:

$$\sigma_{t,1} = \sigma_{t0,1} \quad (3.15)$$

The interlocking is linked to an increment of cohesion as formulated in equation 3.16.

$$c_1 = c_{0,1} + \left(\frac{b}{2a}c_{0,2} + \frac{b}{2a}\sigma_{n,2} \tan \varphi_2 \right) \tan \varphi_1 \quad (3.16)$$

The *Strength Factor Beta* β , which can be computed by equation 3.17, relates the dimensions of the single brick with the cohesion. Parameters of the *Masonry Model* are illustrated in table 3.4.

$$\beta = \tan \varphi \frac{b}{2a} \quad (3.17)$$

Table 3.4: Parameters of the Masonry Jointed Model.

Parameter	Meaning	Unit
γ_{unsat}	Soil unit weight above p.l	kN/m^3
γ_{sat}	Soil unit weight below p.l	kN/m^3
G	Shear modulus	kN/m^2
ν	Poisson's ratio	-
β	Strength factor	-
c_{mc}	Cohesion	kN/m^2
φ_{mc}	Friction angle	$^{\circ}$
ψ_{mc}	Dilatancy angle	$^{\circ}$
σ_{mc}	Tensile strength	kN/m^2
α_1	Dip angle	$^{\circ}$
α_2	Dip direction	$^{\circ}$
c_1	Cohesion	kN/m^2
φ_1	Friction angle	$^{\circ}$
ψ_1	Dilatancy angle	$^{\circ}$
σ_1	Tensile strength	kN/m^2
α_1	Dip angle	$^{\circ}$
α_2	Dip direction	$^{\circ}$
c_2	Cohesion	kN/m^2
φ_2	Friction angle	$^{\circ}$
ψ_2	Dilatancy angle	$^{\circ}$
σ_2	Tensile strength	kN/m^2

3.2.2.A Masonry model simulation

In order to characterize the response of the Masonry model a numerical test was carried out using PLAXIS 2D. Two panels, with and without opening were taken into account. The panels are 1 m high and 0,99 m wide. On the other hand the opening has a dimension of $400 \times 235 \text{ mm}^2$ as can be seen in figure 3.14. The test was repeated with three different sets of parameters. The first one (set a) presents joints along x direction, the second one (set b) along y direction and the last one (set c) presents a first weak direction with α_1 equals to 45° and a second one with α_1 equals to 135° . These last two dip angles are chosen in order to simulate the diagonal frontals on the Pombalino masonry wall. Table 3.5 presents parameters of sets considered. The numerical test carried out in PLAXIS 2D consists in three phases: during the first one zero initial stresses are generated by using the *K0 procedure*, then during phase 1 a vertical uniform load is applied to the top of the panel and to conclude, during phase 2, a uniform line displacement is applied at the top surface. The calculation type for phase 1 and 2 is set to *Plastic*. The boundary condition of the bottom surface was set to *Normally fixed*. The imposed displacement was $1E - 6 \text{ m}$ and the vertical uniform load was 50 kPa . Ground and upper floors of Pombalino are built with different dimensions stone, therefore to simplify we assumed the same value of height and length for each block ($a = b$). As a results, the *Strength Factor Beta* becomes (equation 3.18):

$$\beta = \frac{\tan \varphi}{2} \quad (3.18)$$

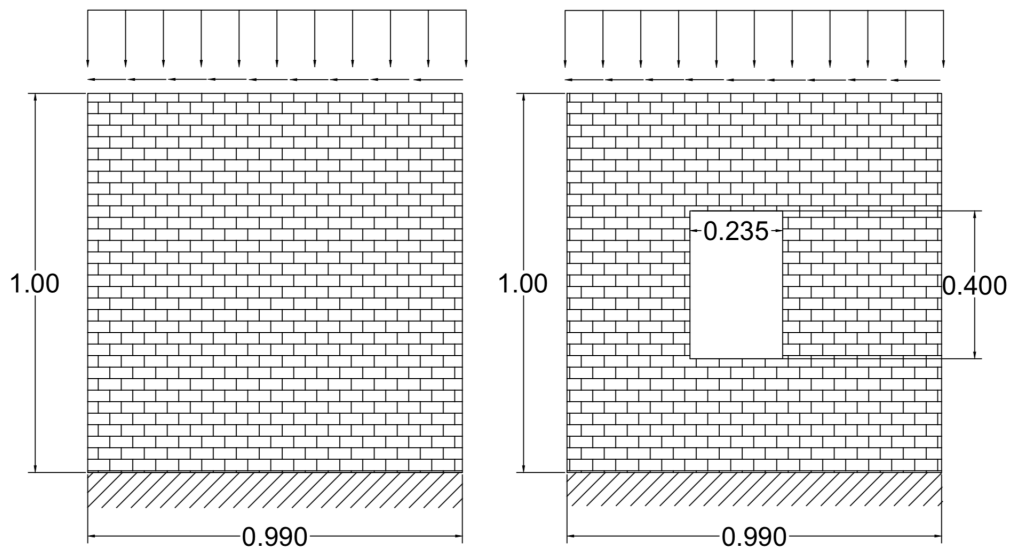
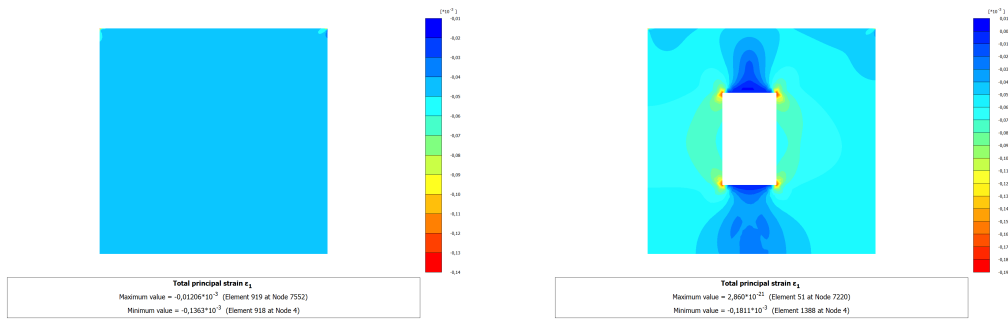


Figure 3.14: Geometry of panels tested. Dimensions are given in meters.

Table 3.5: Parameters of the Masonry Jointed Model for the tests.

Parameter	set <i>a</i>	set <i>b</i>	set <i>c</i>	Unit
γ	20	20	20	kN/m^3
G	410E3	410E3	410E3	kN/m^2
ν	0,2	0,2	0,2	-
β	0,445	0,445	0,445	-
c_{mc}	90	90	90	kN/m^2
φ_{mc}	23,98	23,98	23,98	°
ψ_{mc}	0	0	0	°
σ_{mc}	135,00	135,00	135,00	kN/m^2
α_1	0	90	45	°
α_2	90	90	90	°
c_1	5	90	5	kN/m^2
φ_1	23,98	23,98	23,98	°
ψ_1	0	0	0	°
σ_1	7,5	135,00	7,5	kN/m^2
α_1	0	0	135	°
α_2	90	90	90	°
c_2	90	10	15	kN/m^2
φ_2	23,98	23,98	23,98	°
ψ_2	0	0	0	°
σ_2	135,00	15,00	22,5	kN/m^2

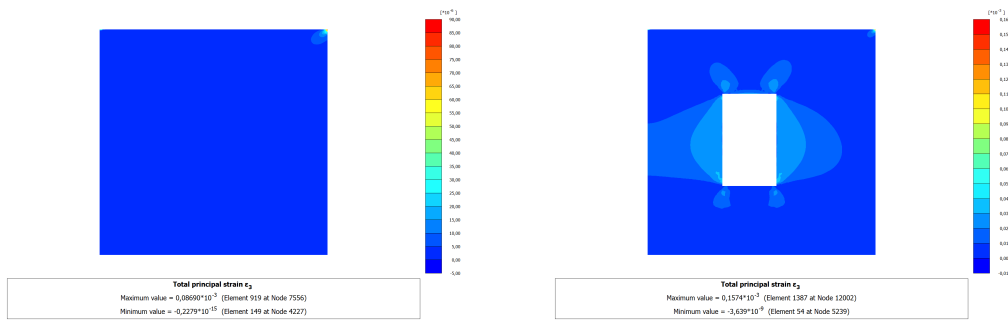
Deformations ε_1 and ε_3 at the end of application of load and horizontal displacements are shown from figures 3.15 to 3.20 respectively for sets *a*, *b* and *c*. It is noticeable that panels without openings do not suffer of considerable deformations. On the other hand panels with openings present different strains concentrations. For every set of parameters considered ε_1 behaves most as a compressive strain (negative) and ε_3 as a tensile strain (positive). They both have a magnitude of $E - 3$ with a peak value in the top right corner of the opening. Sets *a* and *b* clearly show a crack pattern which develops according to the weak directions defined by parameter α_1 and α_2 . Contours of strains ε_1 and ε_3 start from the corners of the opening and develops towards the opposite corner of the wall.



(a)

(b)

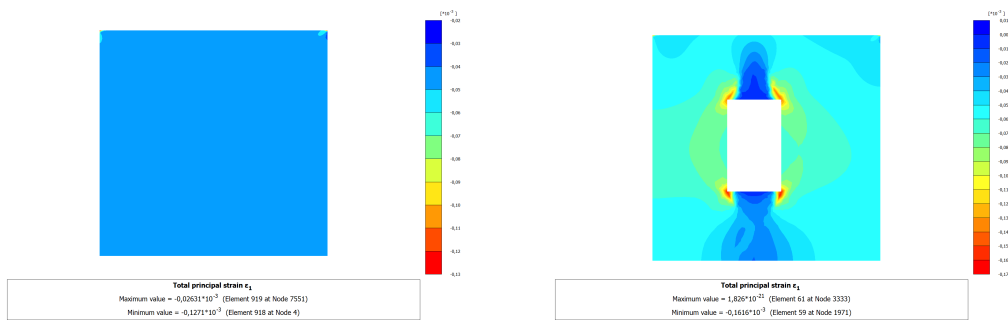
Figure 3.15: Total principal strain ϵ_1 for set a.



(a)

(b)

Figure 3.16: Total principal strain ϵ_3 for set a.



(a)

(b)

Figure 3.17: Total principal strain ϵ_1 for set b.

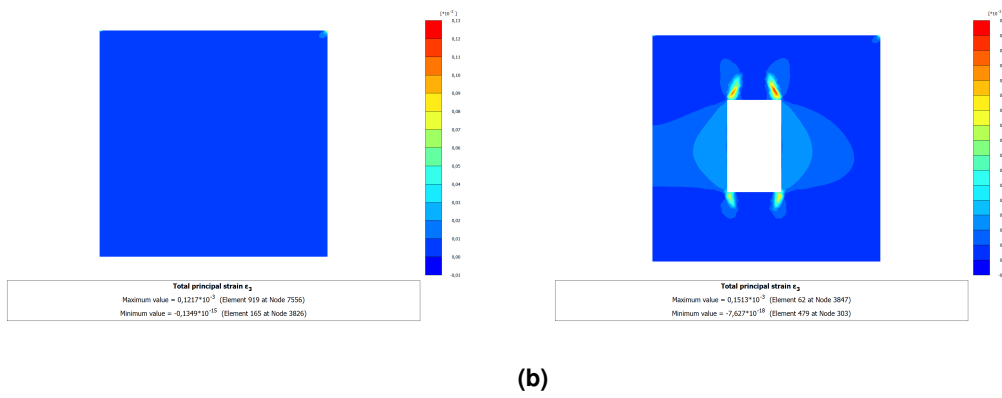


Figure 3.18: Total principal strain ϵ_3 for set b.

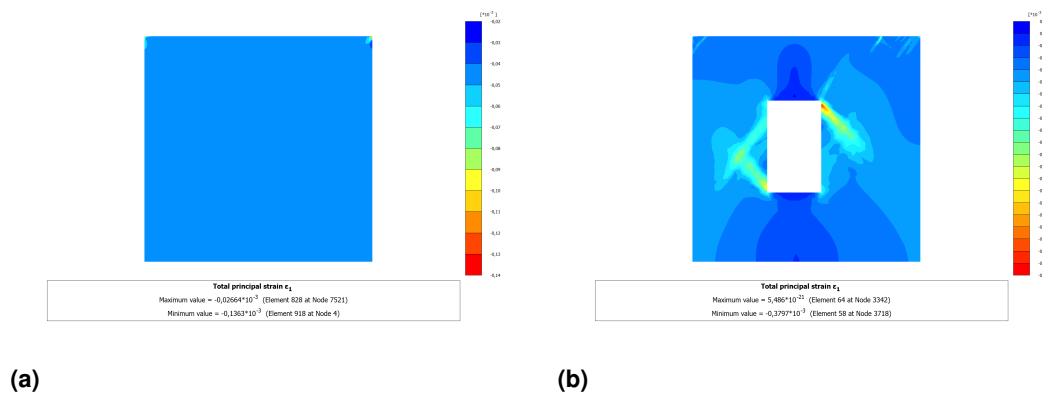


Figure 3.19: Total principal strain ϵ_1 for set c.

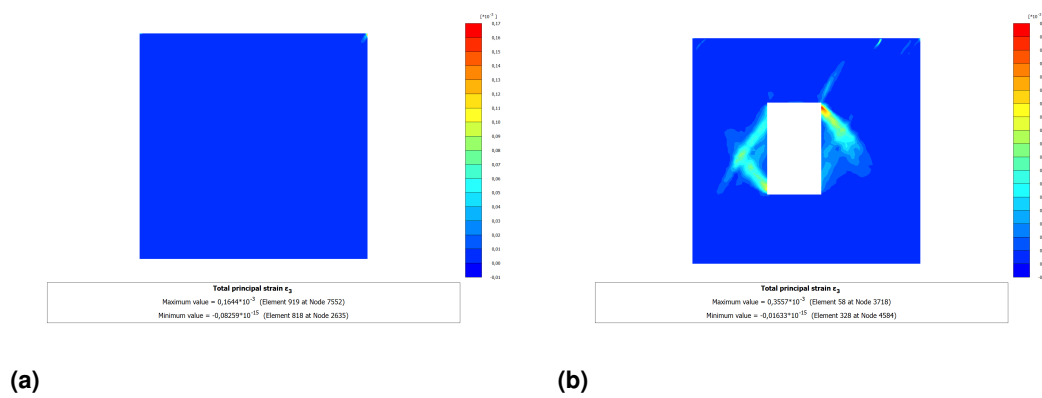


Figure 3.20: Total principal strain ϵ_3 for set c.

3.3 Drainage conditions simulated in PLAXIS 2D

According to Terzaghi's principle, stresses in the soil are divided into effective stresses σ' and pore pressure σ_w :

$$\underline{\sigma} = \underline{\sigma}' + \underline{\sigma}_w \quad (3.19)$$

Pore pressures are generally provided by water in the pores. Water is considered not to sustain any shear stresses. As a result, effective shear stresses are equal to total shear stresses. Moreover, water is considered to be fully isotropic, so all pore pressure components are equal. Hence, pore pressure can be represented by a single value p_w [12].

$$\underline{\sigma} = \underline{\sigma}' + m p_{active} \quad (3.20)$$

where:

$$m = \begin{bmatrix} 1 \\ 1 \\ 1 \\ 0 \\ 0 \\ 0 \end{bmatrix}$$

and

$$p_{active} = \alpha S_e p_w$$

where α is Biot's pore pressure coefficient and S_e is the effective degree of saturation. If we consider incompressible grains, Biot's coefficient is equal to 1. In PLAXIS 2D $\alpha S_e p_w$ is called "Active pore pressure". In addition we can also distinguish between "Initial pore pressure" $p_{initial}$ and "Excess pore stress" p_{excess} :

$$p_w = p_{initial} + p_{excess} \quad (3.21)$$

Initial pore pressures are considered to be input data whereas excess pore pressures are generated during plastic calculations for the case of *Undrained (A)* or *Undrained(B)* material behavior or during a consolidation analysis [12].

It is possible to calculate excess pore pressures. Since the time derivative of the initial component equals zero, it follows:

$$\dot{p}_w = \dot{p}_{excess} \quad (3.22)$$

By inverting Hooke's law in terms of total stress and by using undrained parameters E_u and ν_u it is possible to evaluate excess pore pressures.

$$\begin{bmatrix} \dot{\epsilon}_{xx}^e \\ \dot{\epsilon}_{yy}^e \\ \dot{\epsilon}_{zz}^e \\ \dot{\gamma}_{xy}^e \\ \dot{\gamma}_{yz}^e \\ \dot{\gamma}_{zx}^e \end{bmatrix} = \frac{1}{E_u} \begin{bmatrix} 1 & -\nu_u & -\nu_u & 0 & 0 & 0 \\ -\nu_u & 1 & -\nu_u & 0 & 0 & 0 \\ -\nu_u & -\nu_u & 1 & 0 & 0 & 0 \\ 0 & 0 & 0 & 2 + 2\nu_u & 0 & 0 \\ 0 & 0 & 0 & 0 & 2 + 2\nu_u & 0 \\ 0 & 0 & 0 & 0 & 0 & 2 + 2\nu_u \end{bmatrix} \begin{bmatrix} \dot{\sigma}_{xx} \\ \dot{\sigma}_{yy} \\ \dot{\sigma}_{zz} \\ \dot{\sigma}_{xy} \\ \dot{\sigma}_{yz} \\ \dot{\sigma}_{zx} \end{bmatrix} \quad (3.23)$$

Where:

$$E_u = 2G(1 + \nu_u) \quad (3.24)$$

$$\nu_u = \frac{3\nu' + \alpha B(1 - 2\nu')}{3 - \alpha B(1 - 2\nu')} \quad (3.25)$$

where B is Skempton's B-parameter.

$$B = \frac{\alpha}{\alpha + n\left(\frac{K'}{K_w} + \alpha - 1\right)} \quad (3.26)$$

According to equations (3.24) and (3.25) is possible to transform G and ν' into E_u and ν_u . In order to avoid numerical problems caused by an extremely low compressibility ν_u is by default taken as 0,495. Moreover to ensure realistic computational results is considered $\nu' < 0,35$ [12].

For material behaviour *Undrained(A)* or *Undrained(B)* a bulk modulus for water is automatically considered in the stiffness matrix. Alternately the user can specify the value of the bulk stiffness of water otherwise it is added automatically by the following equation:

$$\frac{K_w}{n} = \frac{3(\nu_u - \nu')}{(1 - 2\nu_u)(1 + \nu')} K' \quad (3.27)$$

where K' is the effective bulk modulus of the soil matrix and K_s is the bulk modulus of the solid material. n is the porosity:

$$n = \frac{e_0}{1 + e_0} \quad (3.28)$$

3.3.1 Drained and undrained analysis

In this thesis, it is assumed that, considering the relatively low permeability of the alluvium soil layer, the water level drawdown occurs at a very low rate, possibly along several years or even decades. To simulate this in a easy manner, without increasing tremendously the computation time, the analysis was performed in *drained conditions* varying the position of the water level from the initial position to the lowest level. In this simplified manner, equilibrium for each intermediate step was verified.

3.4 2D Model

In this section the 2D model implemented in PLAXIS 2D is explained in detail. Two different cases were considered with the aim of simulate in a soil deposit displacements due to the decrease of water table.

3.4.1 Ground model

3.4.1.A Geometry

A soil deposit of 25,0 *m* thickness is considered. It is composed by three layers (table 3.6): the upper layer (ZG1), representative of a backfill, goes from a depth of 0 to 1,5 *m*, the middle layer (ZG2), representative of alluvium deposit, goes from 1,5 to 10 *m* and the bottom layer (ZG3), representative of miocene deposit, goes from 10 to 15 *m*. Under ZG3 is situated a stiff rock layer that extends to a large depth and it is not included in the model. The geometry of the model is showed in figure 3.21.

The goal is to study displacements and stresses diel caused by the decrease of watertable. To simulate the variation of water level in PLAXIS 2D five different phases were taken into account. At the initial phase the water table is stable at 22 *m*. During each phase a drawdown of 1 *m* is considered. At the end of calculation (phase 5) the water table is stable at 17 *m*.

Table 3.6: Soil layers in Restauradores square.

Layer	Depth (<i>m</i>)	Thickness (<i>m</i>)
ZG1	0 - 1,5	1,5
ZG2	1,5 - 10	8,5
ZG3	10 - 25	15

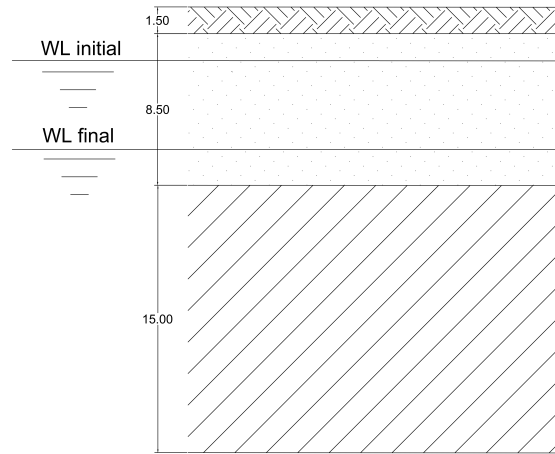


Figure 3.21: Geometry of the model without underground structure.

3.4.1.B Properties

Hardening Soil with small-strain stiffness model describes well the behaviour of Lisbon downtown soil as studied by Silva [11]. Parameters chosen for the simulation (tables 3.7 and) come from the *GeoSIS.Lx* research project promoted by the Municipality of Lisbon. In these simulations, it is assumed that, considering the relatively low permeability of the alluvium soil layer, the water level drawdown occurs at a very low rate, possibly along several years or even decades. To simulate this in a easy manner, without increasing tremendously the computation time, the analysis was performed in drained conditions varying the position of the water level from the initial position to the lowest level.

Table 3.7: Parameters of *ZG1* with Mohr Coulomb model.

Parameter	Meaning	Value	Unit
Type	Drainage type	Drained	-
γ_{unsat}	Soil unit weight above p.l.	17,6	kN/m^3
γ_{sat}	Soil unit weight below p.l.	17,6	kN/m^3
E'	Young's modulus (constant)	8,3E3	kN/m^2
ν'	Poisson's ratio	0,3	-
c'_{ref}	Cohesion	0	kN/m^2
φ'	Friction angle	27	$^\circ$
ψ	Dilatancy angle	0	$^\circ$

Table 3.8: Parameters of ZG2 and ZG3 with Hardening Soil with small-strain stiffness model.

Parameter	Meaning	ZG2	ZG3	Unit
<i>Type</i>	Drainage type	Drained	Drained	-
γ_{unsat}	Soil unit weight above p.l.	17,6	18,5	kN/m^3
γ_{sat}	Soil unit weight below p.l.	17,6	18,5	kN/m^3
c'_{ref}	(Effective) cohesion	0,00	0,00	kN/m^2
φ'	(Effective) angle of internal friction	29,00	35,00	°
ψ	Dilatancy angle	0,00	0,00	°
E_{50}^{ref}	Secant stiffness in standard drained triaxial test	125,0E3	250,0E3	kN/m^2
E_{oed}^{ref}	Tangent stiffness for primary oedometer loading	125,0E3	250,0E3	kN/m^2
E_{ur}^{ref}	Unloading / reloading stiffness	145,0E3	750,0E3	kN/m^2
<i>m</i>	Power for stress-level dependency of stiffness	0,5	0,8	
$\gamma_{0.7}$	Shear strain at which $G_s = 0.722G_0$	0,3E-3	1,0E-4	
G_0^{ref}	Shear modulus at very small strains	145,0E3	300,0E3	kN/m^2
ν'	Poisson's ratio	0,3	0,25	-
k_x	Horizontal permeability	1,56E-5	1,45E-4	<i>m/day</i>
k_y	Vertical permeability	1,56E-5	1,45E-4	<i>m/day</i>
<i>type</i>	Interface strength type	Rigid	Rigid	-
R_{inter}	Interface strength	1,0	1	-
	K_0 determination	Manual	Manual	-
$k_{0,x}$	Lateral earth pressure coefficient	0,5	0,67	-
<i>OCR</i>	Over-consolidation ratio	1,0	1,0	-
<i>POP</i>	Pre-overburden ratio	0,0	0,0	-

3.4.1.C Results

The maximum total displacement at the end of calculation is equal to 2,975 *mm* and it is reached at the top surface of the soil deposit as showed in figure 3.23. Its horizontal component is negligible, so it develops downward. Figure 3.22 illustrates the trend of effective vertical and horizontal stresses at the end water drawdown. According to the linear elasticity theory equations 3.29 and 3.30 allow to calculate one dimensional settlement for a soil layer:

$$\Delta\varepsilon = \frac{\Delta\sigma'}{E} \quad (3.29)$$

$$\Delta h = \Delta\varepsilon \cdot h \quad (3.30)$$

Considering ZG1 which has a thickness of 1,5 *m* and a Young's modulus of 8,3E3 *kPa* the settlement calculated results to have a magnitude of *mm* as computed by PLAXIS 2D.

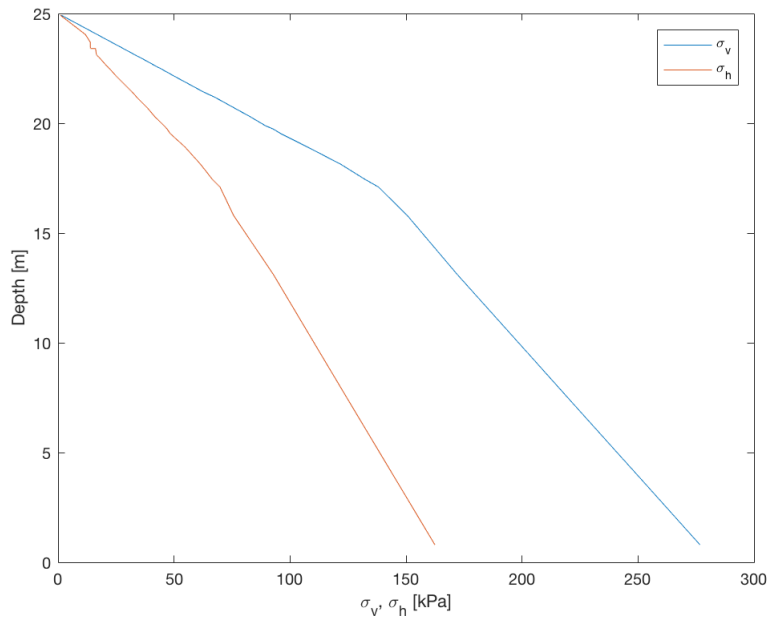


Figure 3.22: Principal vertical effective stress (blu) and principal horizontal effective stress (orange) at the end of water drawdown.

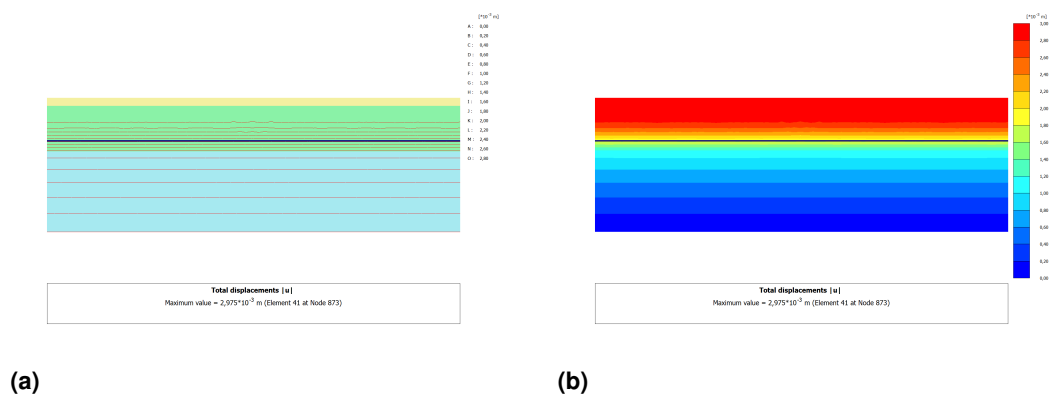


Figure 3.23: Shadings (right) and contour lines (left) of total displacement at the end of calculation.

3.4.2 2D with underground structure

3.4.2.A Geometry

In this case the geometry of soil layers and their parameters are the same of the previous case (tables 3.7 and 4.3). An underground structure 30 m long and 8 m deep is installed in the center of the model. The side and the base of the structure are supported by diaphragm walls which ensure they are impervious. The geometry of the model is showed in figure 3.24. To simulate the pumping of water from the excavation, five different phases are taken into account. During each phase a drawdown of 1 m is considered as in the previous case. At the end of phase 5 there is no presence of water at the base of excavation. The drawdown was computed by PLAXIS 2D by creating at each phase a new water table. The shape of water level during drawdown was determined using settlement contours. In conclusion, in order to investigate the effects of a possible drawn up of the water table, a new phase is added. In this phase the water table rises up to the original level (22 m). The shape of water level during water drawdown was determined using settlement contours

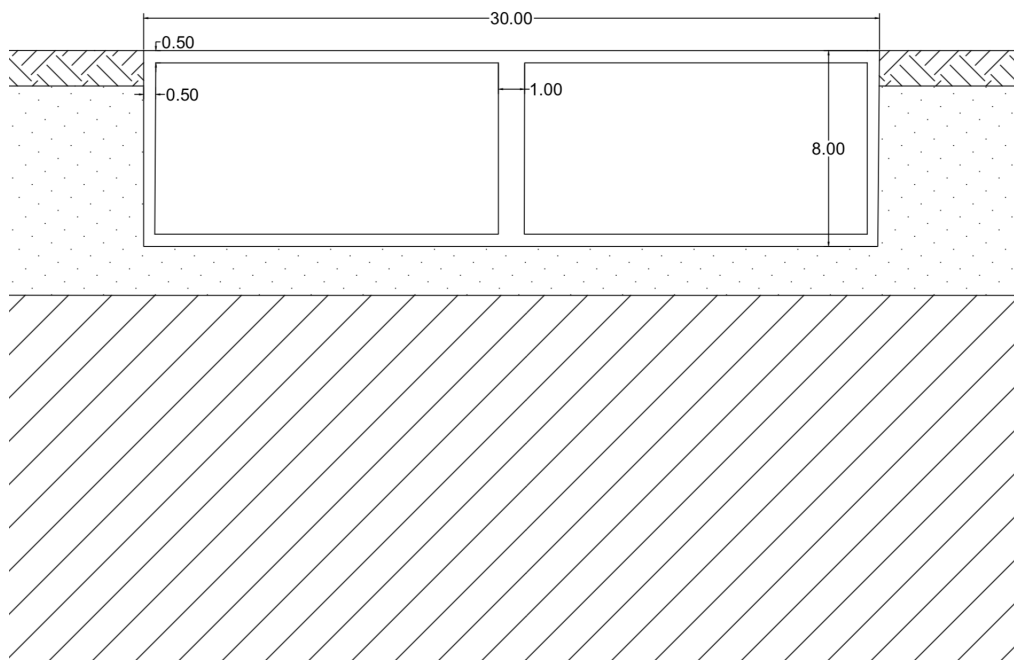


Figure 3.24: Geometry of the model with underground structure.

3.4.2.B Properties

Properties of layers ZG1, ZG2 and ZG3 are the same of tables 3.7 and 4.3. In this study the construction of the wall is not taken into account, hence parameters of diaphragm wall were chosen in order to guarantee that it was sufficiently rigid. Table 3.9 contains parameters of the wall.

Table 3.9: Material properties of the diaphragm wall.

Parameter	Name	Value	Unit
Material type	Type Elastic; Isotropic		-
Normal stiffness	EA	12E+06	kN/m
Flexural rigidity	EI	1,8E+06	kNm^2/m
Weight	w	10,00	kNm^2/m
Poisson's ratio	ν	0,00	-

3.4.2.C Results

In order to investigate the effects of water level decrease on displacements at surface the option *Reset displacements to zero* was selected after the phase of parking area activation. Figures 3.26, 3.27 and 3.28 show trends of displacements at each calculation phase in the surroundings of the parking area, more precisely on the left side of excavation from $x = 55,89 \text{ m}$ to $x = 67,74 \text{ m}$. Settlements due to the decrease of water level are correspond to parallel curves that develop gradually upward. Curve *installation* represents displacements due to the activation of the self weight of the building and curve *rise* is the curve of settlements induced by the rise of water level.

Figure 3.32 allows to relate each line displacement to the respective water drawdown. A maximum total displacement corresponding to $2,64E - 3 \text{ m}$ is reached at phase 5 when the drawdown is completed. This value is comparable with the maximum displacement obtained after the activation of the parking area, but they follow a different path. Figure 3.29 illustrates the deformed mesh after the water drawdown. It exhibits deformations which follow the same trend described by settlements due to the decrease of water level. Moreover figure 3.28 shows that settlements due to the rise up of water level (black curve) do not induce remarkable effects. Figure 3.31 shows a narrow representation of total displacement. It is evident that settlements are influenced by the activation of the parking area and progressively by the water level decrease.

Figure 3.32 illustrates how water pressure varies consistently with the water table levels assigned in PLAXIS 2D in the *Flow condition* section. Finally figure 3.33 is a sequence of shading maps representing the evolution of total displacements. Settlements due to the activation of the parking area develop under the central part of the construction. On the other hand settlements due to the water lowering gather from $x = 55,5 \text{ m}$ to $x = 61,3 \text{ m}$ and from surface up to a depth of 5 m . Their magnitude dissipates slower going toward $x = 0$ rather than toward the wall.

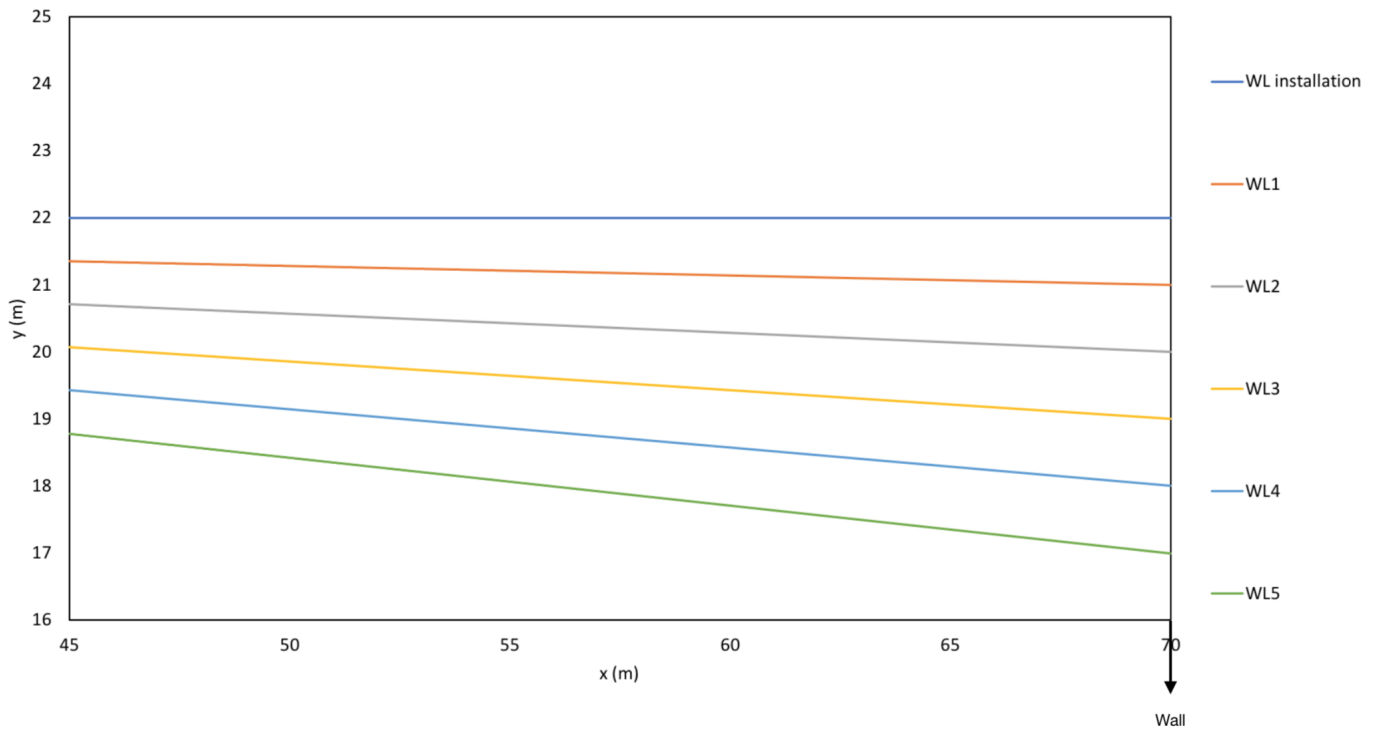


Figure 3.25: Evolution of water drawdown surrounding the parking area.

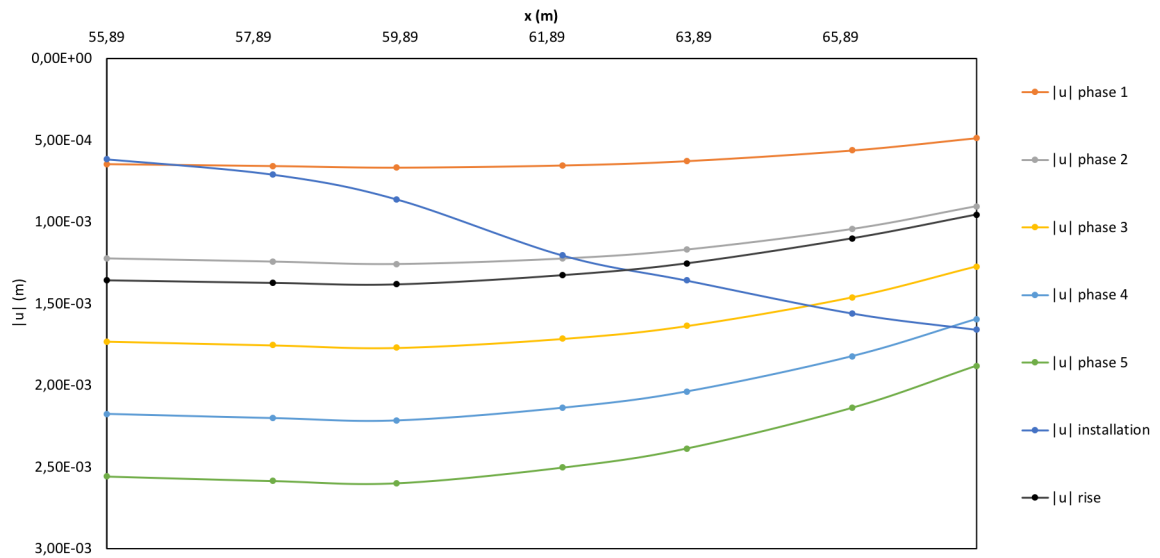


Figure 3.26: Evolution of total displacements surrounding the parking area.

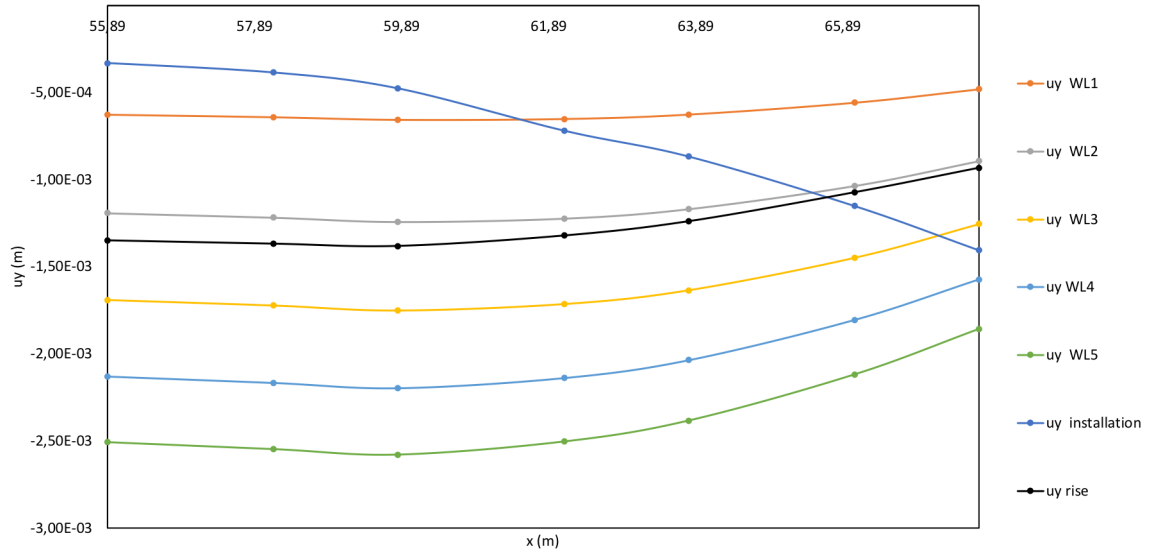


Figure 3.27: Evolution of vertical displacements surrounding the parking area.

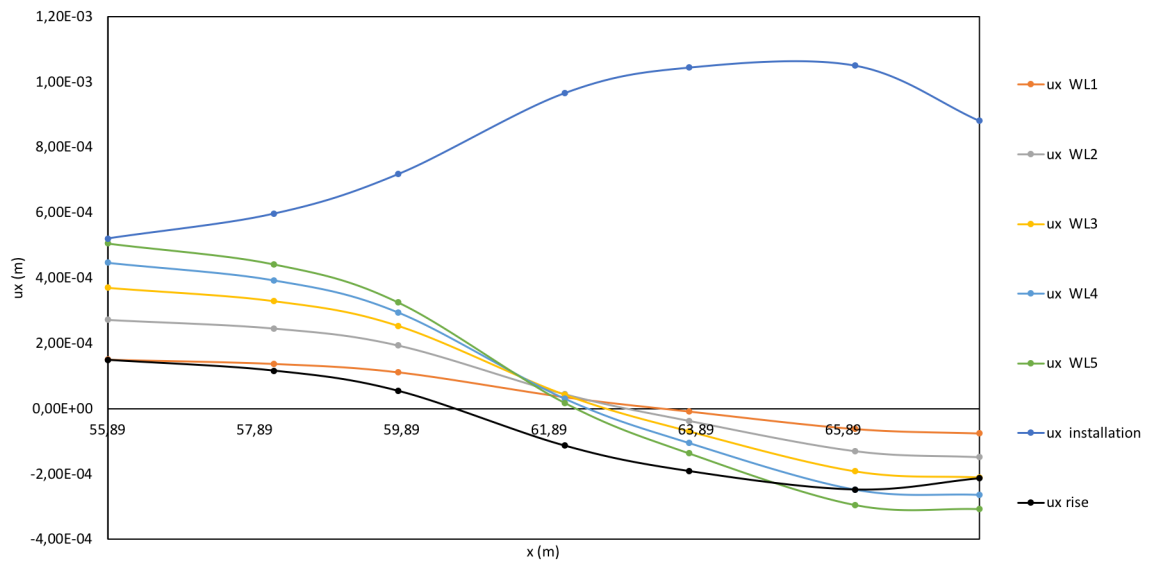


Figure 3.28: Evolution of horizontal displacements surrounding the parking area.

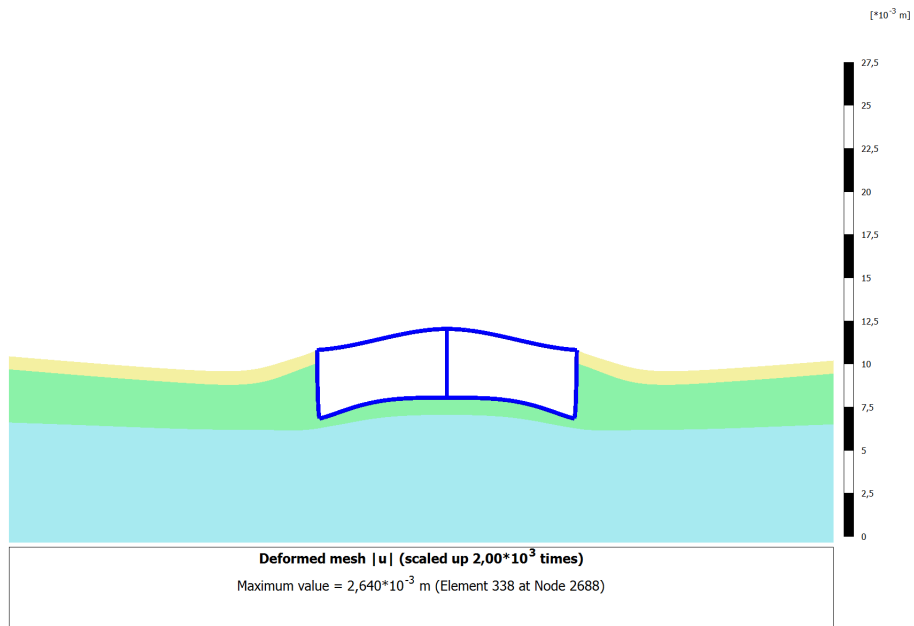


Figure 3.29: Deformed mesh at the end of calculation.

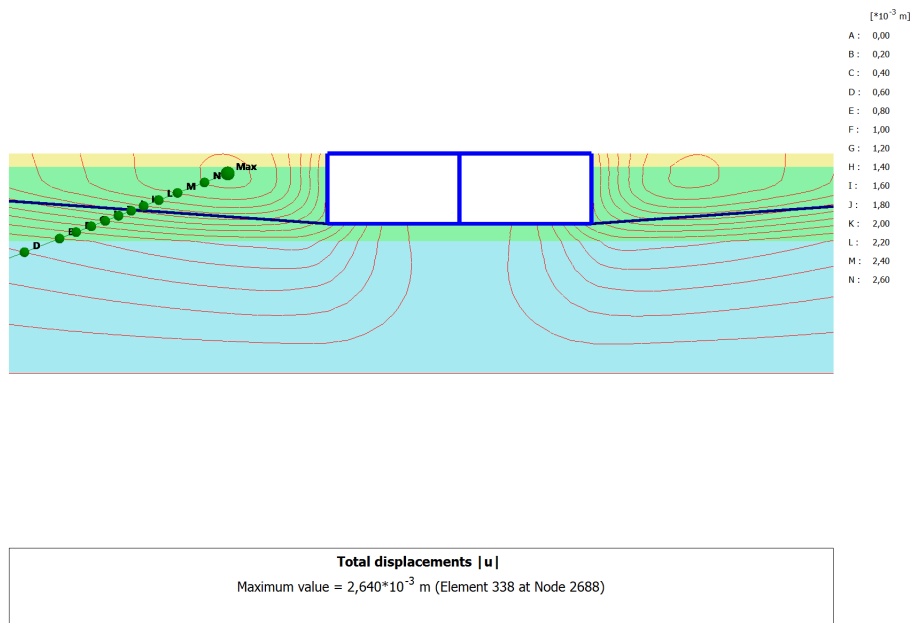


Figure 3.30: Contour lines of total displacements at the end of water drawdown.

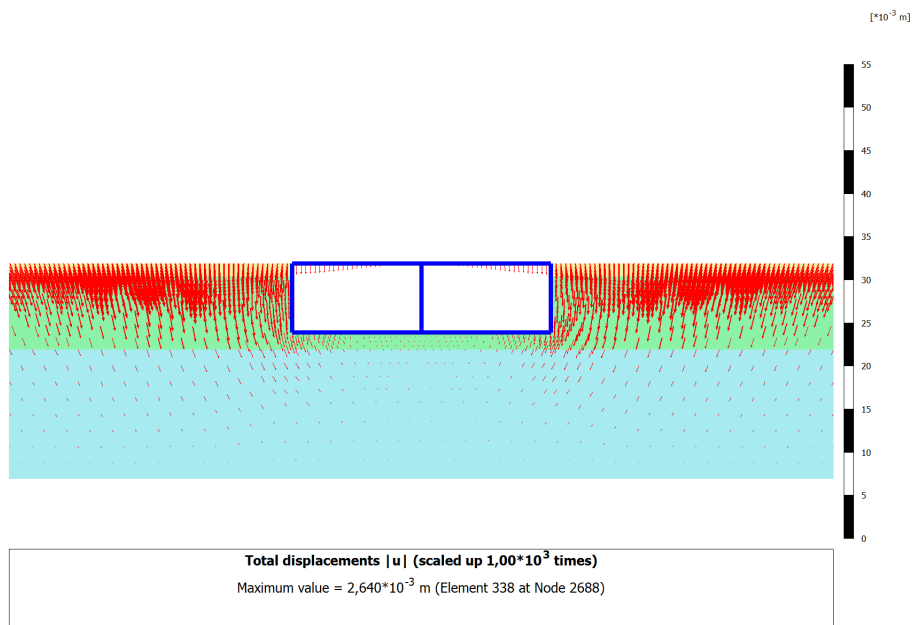


Figure 3.31: Arrows of total displacements at the end of water drawdown.

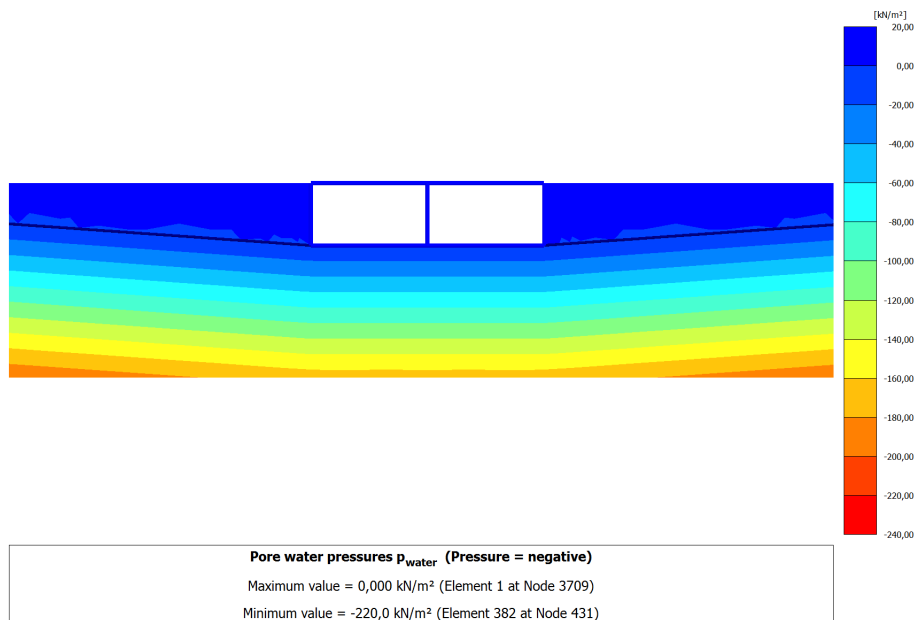
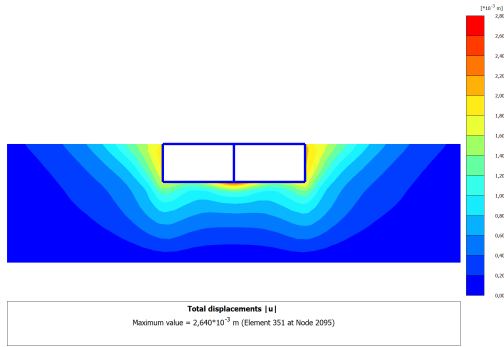
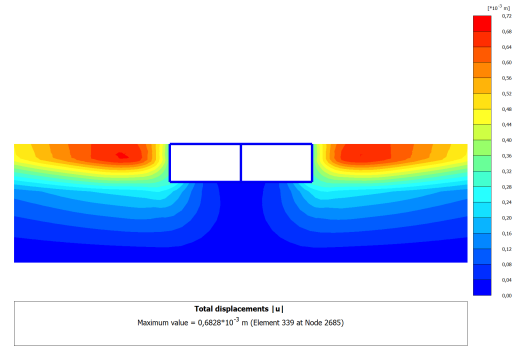


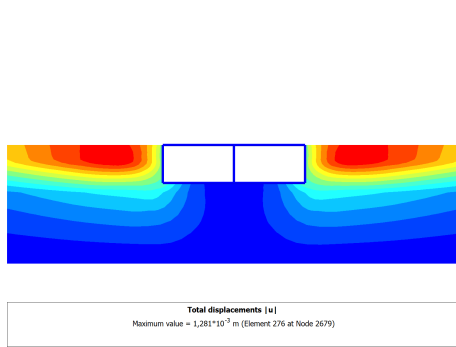
Figure 3.32: Water pressure at the end of calculation.



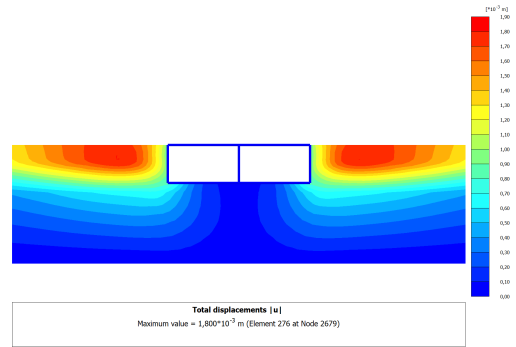
(a)



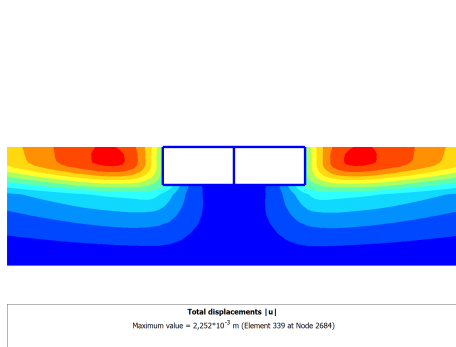
(b)



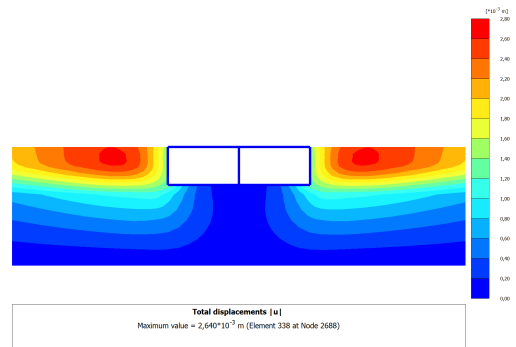
(c)



(d)



(e)



(f)

Figure 3.33: Evolution of total displacements.

4

Case study

Contents

4.1 Modeling Pombalino facade	57
4.2 Drawdown of water level	61
4.3 Results	63

In this chapter is presented the case study of a Pombalino edge located 2 m far from an excavation. Pombalino building and soil models are described in detail in the following section.

4.1 Modeling Pombalino facade

4.1.1 Geometry of Pombalino facade

The Pombalino building chosen was characterized by Renda [6], therefore a large amount of data is available. The building simulated extends horizontally for 17,96 m and it has a total height of 15 m from the surface. It presents a ground floor 4,5 m high and three upper floors with an height of 3,5 m each. Each floor has six parallel openings with different dimensions. The foundation system simulated is made by a slab of 1 m thick and seven timber piles 2 m long. The ground floor and the foundation system consist of walls and columns in stone masonry. The upper floors are built in ordinary masonry. Figure 4.1 illustrates the geometry of the facade simulated. It is possible to note the main differences with the real facade of Pombalino building as the absence of roof and wooden piles.

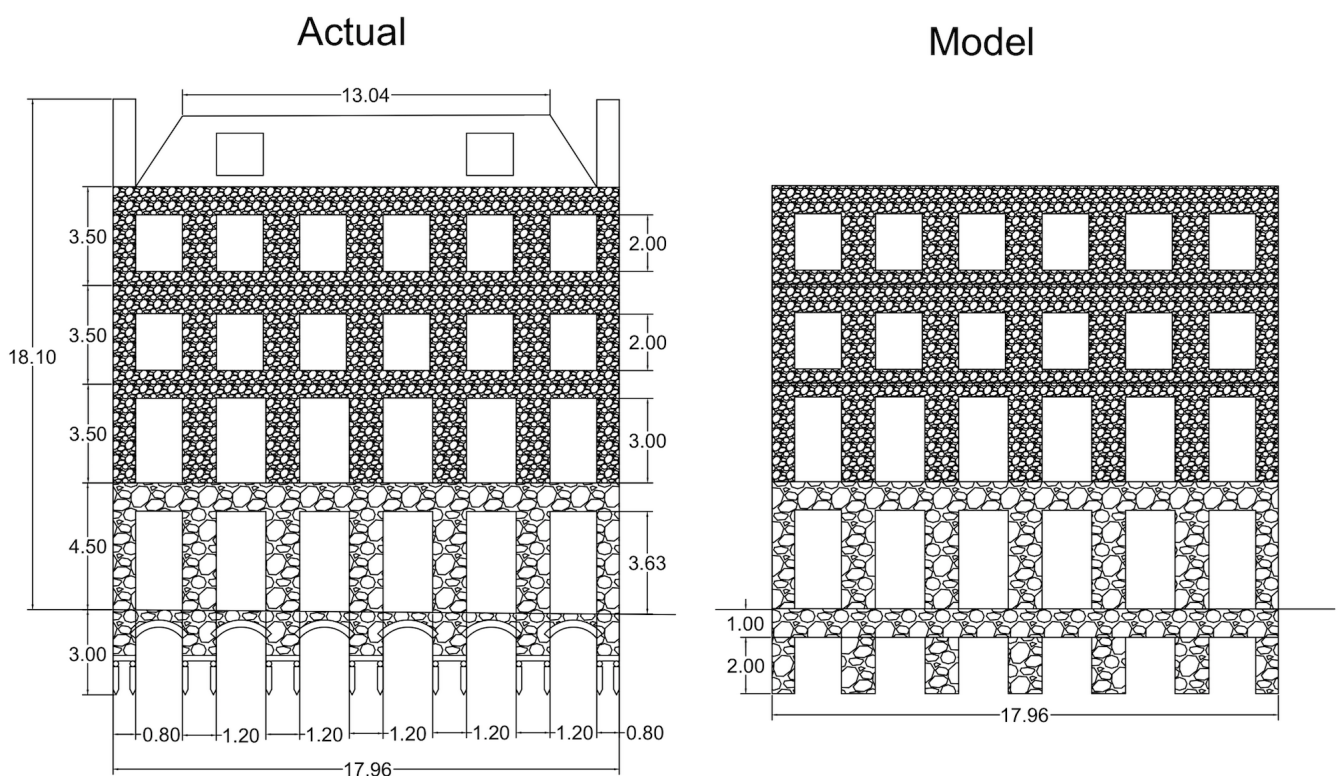


Figure 4.1: Geometry of the real Pombalino building studied (left), and building simulated in PLAXIS 2D (right).

4.1.2 Properties of Pombalino facade

In PLAXIS 2D Pombalino building was simulated with two different material models: foundations and ground floors with Mohr-Coulomb model, externals upper walls with Masonry Model, in which an horizontal weak direction is selected in order to take into account the orientation of laying stones. In Pombalino buildings frontal timber crosses were installed about 200 years ago to respond to earthquake motion, but now they are particularly degraded, especially at the connections. They became weak directions that cross each other with a dip angle of 45° and 135° (figure 4.2). The area between frontals is filled by masonry built by stones with smaller dimensions than the ones of the ground floor. In order to reproduce this constructive elements a Masonry model was assigned to the openings and two joint families were selected and oriented as the wooden frontals. The same value of height and length was considered for each masonry block ($a = b$), therefore β is expressed by equation 3.18, due to the randomness of the size and orientation of ordinary masonry.

Parameters of ground floor, slab and piles are presented in table 4.1. Their values are provided by the Italian regulations NTC 2008 applying the drawdown factor of 50 % for Young modulus and shear modulus. Parameters of upper floors were obtained thanks to experimental works developed by Santos (1997) in old buildings that were later demolished [6]. These latter are contained in table 4.2.

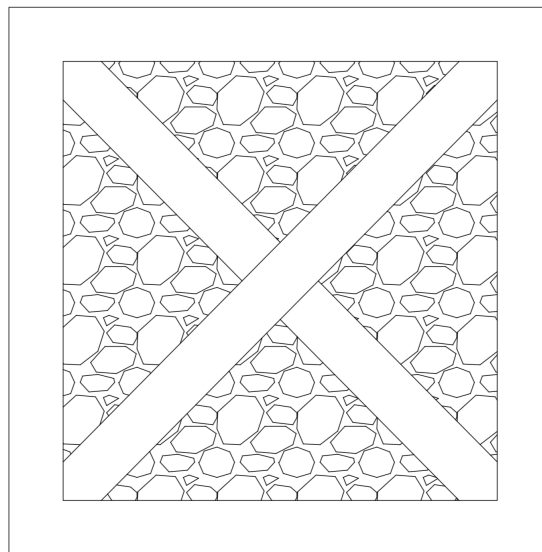


Figure 4.2: Example of Pombalino wall with frontals.

Table 4.1: Parameters of Pombalino building foundations and ground floor.

Parameter	Value	Unit
Material Model	Mohr-Coulomb Model	
γ	22	kN/m^3
G	430E3	kN/m^2
E'	1,032E6	kN/m^2
ν'	0,2	-
c'_{ref}	140	kN/m^2
φ'	23,98	°
ψ	0	°

Table 4.2: Parameters of Pombalino building upper floors.

Parameter	Value	Unit
Material Model	Masonry Model	
γ	20	kN/m^3
G	410E3	kN/m^2
ν	0,2	-
β	0,445	-
c_{mc}	90	kN/m^2
φ_{mc}	23,98	°
ψ_{mc}	0	°
σ_{mc}	135,00	kN/m^2
α_1	0	°
α_2	90	°
c_1	5	kN/m^2
φ_1	23,98	°
ψ_1	0	°
σ_1	7,5	kN/m^2

4.1.3 Soil profile

The soil deposit considered consists of three layers with a total thickness of 25,0 *m*. The upper layer (ZG1) representative of a fill and goes from a depth of 0 to 1,5 *m*. The middle layer (ZG2) is the alluvium layer and goes from 1,5 to 10 *m*. The bottom layer (ZG3) is the miocene layer and goes from 10 to 15 *m*. Under ZG3 is situated a very stiff soil layer that extends to a large depth and it is not included in the model. The excavation is carried out from 70 to 100 *m* up to a depth of 17 *m*. Pombalino is located 2 *m* far from one side of the excavation. Figures 4.3 and 4.4 show respectively the geometry of the case study and the mesh generated by PLAXIS 2D. This latter is created with the command *fine elements*

and it is composed by 1540 soil elements and 12685 nodes. The average element size is 2,168 *m*, the maximum 8,009 *m* and the minimum 0,5 *m*.

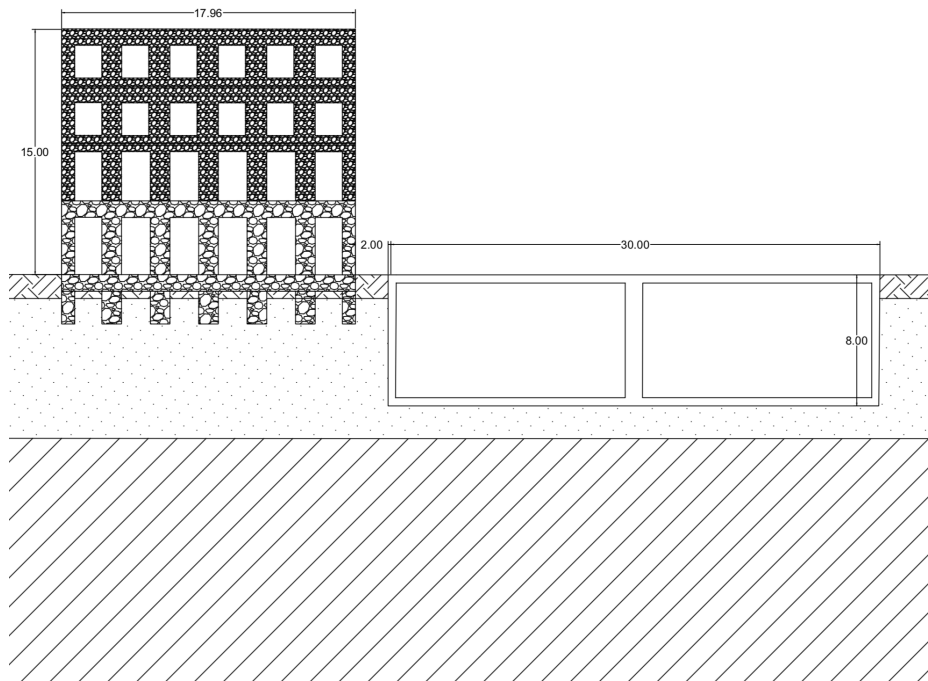


Figure 4.3: Geometry of the case study.

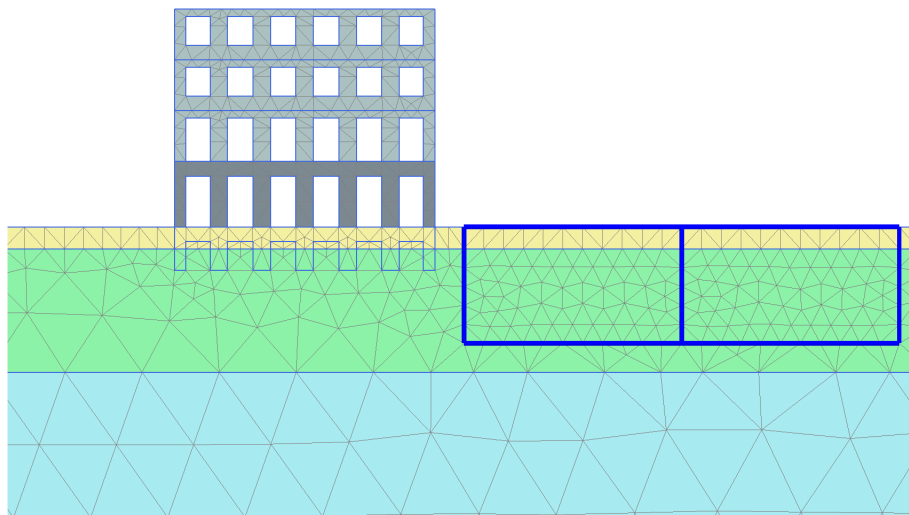


Figure 4.4: The generated mesh for the case study.

4.1.4 Soil properties

Parameters of soil layers are the same of study cases developed in chapter 3 and they are presented in tables 3.7 and 4.3. Also parameters of diaphragm wall are the same of previous case (table 3.9). In PLAXIS 2D the layer ZG1 was modeled with a Mohr-Coulomb model because the deformation in this layer is not so relevant for the global response of the model. On the other hand the Hardening Soil with small-strain stiffness model was used for ZG2 and ZG3. This numerical model can simulate more accurately stiffness in the small strain range. In our case study the water level drawdown induces small to moderate stress variation, so it is important to simulate well the small strain stiffness. Hardening Soil with small-strain stiffness model requires to define for each layer two additional parameters which describe the behaviour of stiffness in the range of small deformations (G_0) and the rate of stiffness degradation ($\gamma_{0.7}$). With equation 4.1 is possible to compute the maximum shear modulus G_0 :

$$G_0 = \rho \cdot V_s^2 \quad (4.1)$$

where:

$$\rho = \frac{\gamma}{g} \quad (4.2)$$

Knowing values of γ for layers ZG2 and ZG3 is possible to obtain values of G_0 and the Young modulus through equation 4.3:

$$E = 2G(1 + \nu) \quad (4.3)$$

Finally equation 3.8 was implemented to compute the stiffness degradation curve. The value of deformations corresponding to $G/G_0 = 0,7$ is the second additional parameter needed in the HS small model.

4.2 Drawdown of water level

Pombalino building is a structure built after the earthquake of 1755. In the early 1990's, several excavations to install underground parking area were done in Baixa, with pumping systems active during construction and on service. Only the water level drawdown is considered. In other words the action of the pumping system used to drawdown water table is simulated by drawing a new water level at each phase and by assuming it as the new *Global Water Table*. As explained in chapter 2, the monitoring campaign performed on request of the Municipality of Lisbon extended from 2004 to 2010. Thus this thesis intends to characterize the impact of water table drawdown on surface displacements and if this settlements can explain the damage pattern observed in Pombalino buildings. Moreover, in order to investigate the effect of the rise of water table, another phase in which water level increases is considered.

Table 4.3: Parameters of ZG2 and ZG3 with Hardening Soil with small-strain stiffness model.

Parameter	Meaning	ZG2	ZG3	Unit
$Type$	Drainage type	Drained	Drained	-
γ_{unsat}	Soil unit weight above p.l.	17,6	18,5	kN/m^3
γ_{sat}	Soil unit weight below p.l.	17,6	18,5	kN/m^3
c'_{ref}	(Effective) cohesion	0,00	0,00	kN/m^2
φ'	(Effective) angle of internal friction	29,00	35,00	°
ψ	Dilatancy angle	0,00	0,00	°
E_{50}^{ref}	Secant stiffness in standard drained triaxial test	125,0E3	250,0E3	kN/m^2
E_{oed}^{ref}	Tangent stiffness for primary oedometer loading	125,0E3	250,0E3	kN/m^2
E_{ur}^{ref}	Unloading / reloading stiffness	145,0E3	750,0E3	kN/m^2
m	Power for stress-level dependency of stiffness	0,5	0,8	
$\gamma_{0.7}$	Shear strain at which $G_s = 0.722G_0$	0,3E-3	1,0E-4	
G_0^{ref}	Shear modulus at very small strains	145,0E3	300,0E3	kN/m^2
ν'	Poisson's ratio	0,3	0,25	-
k_x	Horizontal permeability	1,56E-5	1,45E-4	m/day
k_y	Vertical permeability	1,56E-5	1,45E-4	m/day
$type$	Interface strength type	Rigid	Rigid	-
R_{inter}	Interface strength	1,0	1	-
	K_0 determination	Manual	Manual	-
$k_{0,x}$	Lateral earth pressure coefficient	0,5	0,67	-
OCR	Over-consolidation ratio	1,0	1,0	-
POP	Pre-overburden ratio	0,0	0,0	-

In PLAXIS 2D the first calculation stage is set to *K0 procedure*. Pombalino and the excavation are simultaneously activated from the beginning. During phase 1 the water table is stable and the effects of the installation of Pombalino and excavation are taken into account. From phase 2 to phase 6, five water table decreases of 1 m each occur in the area excavated. The water depression cone simulated in PLAXIS 2D is drawn linearly with the command *New water level*. Boundary conditions are set to *free* for Y_{max} , *fixed* for Y_{min} , X_{max} and X_{min} .

4.3 Results

Figure 4.5 shows contour lines of total displacements after the activation of structures (left) and at the end of water drawdown (right). In the first case the maximum displacement is 1 *cm* and it is localized under last right opening of Pombalino in the *ZG1* layer. In the second case the maximum displacement is 2,2 *mm* and is situated in *ZG2* layer to the right of the excavation. In PLAXIS 2D the option *Reset displacement to zero* was selected with the aim to evaluate displacements dues to self weight of structure and to the water decrease. Separately figure 4.6 illustrates the orientation of total displacements in the two phases. Is noticeable that in the first case (figure 4.6 a) two sets displacements can distinguished: the first and the second piles show displacement oriented downward to negative values of coordinate *x*. Starting from $x = 55,5 \text{ m}$ (third foundation pile) the orientation of total displacements is influenced by the soil excavated and changes direction to positive *x* values. On the other hand total displacements induced by the decrease of water level show a similar trend but less evident (figure 4.6 b).

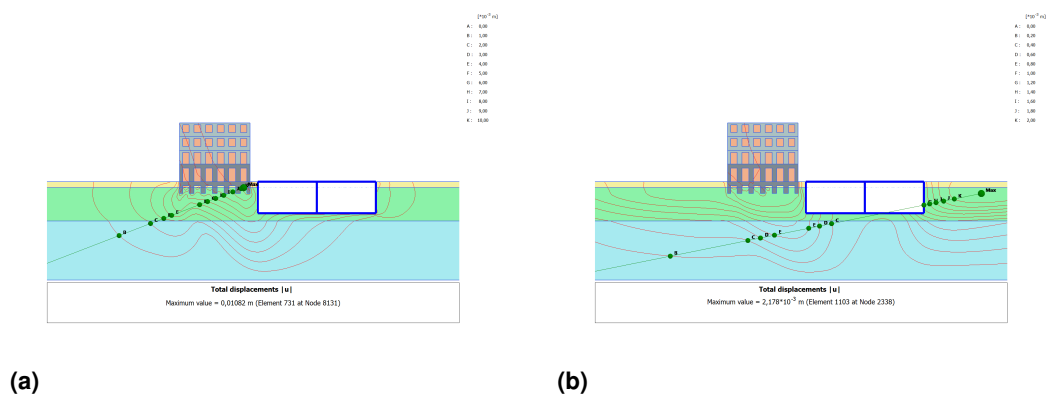


Figure 4.5: Contour lines of total displacements after the Pombalino and parking area activation (left) and at the end of water level drawdown (right).

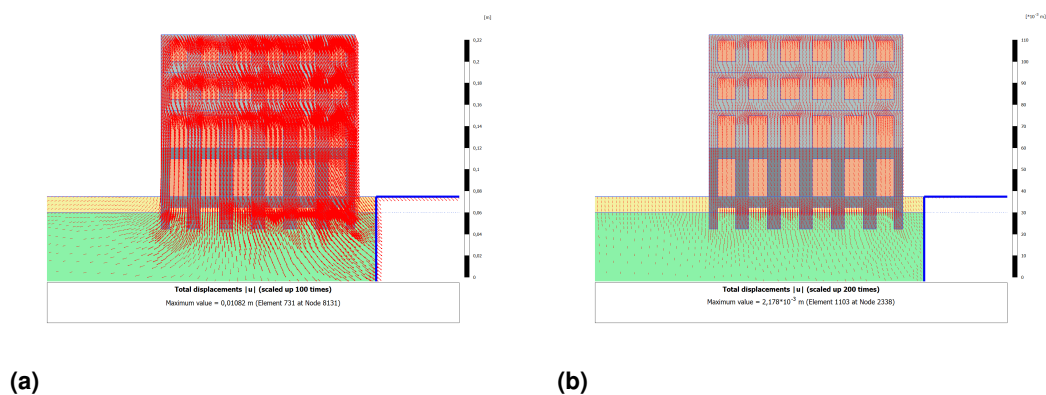
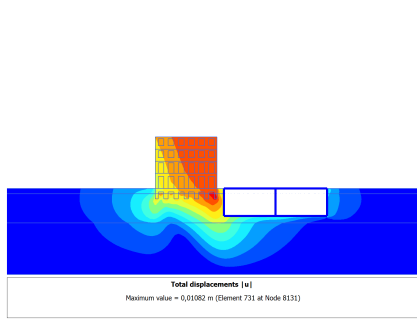
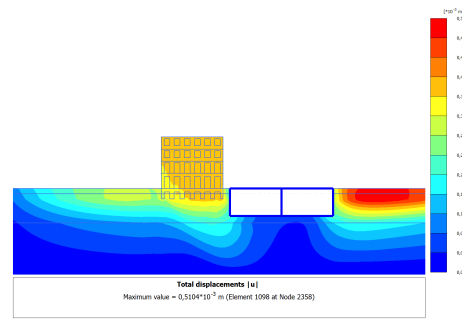


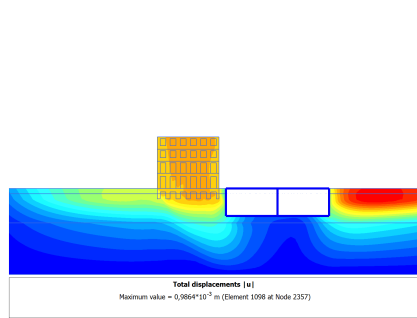
Figure 4.6: Arrows of total displacements after the Pombalino and parking area activation (left) and at the end of water level drawdown (right).



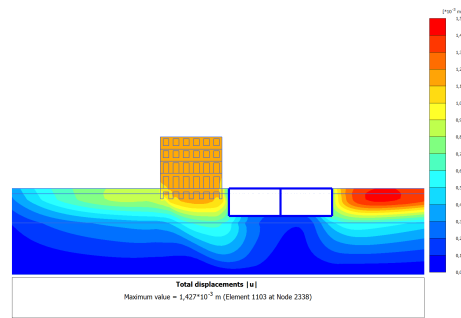
(a)



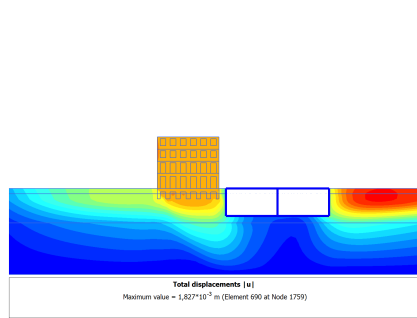
(b)



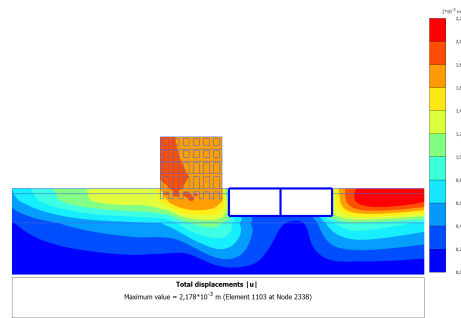
(c)



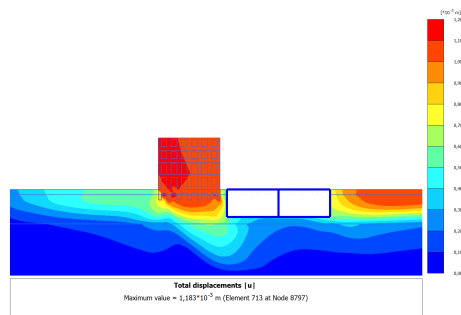
(d)



(e)



(f)



(g)

Figure 4.7: Evolution of total displacements in the entire domain.

Figure 4.7 shows the evolution of total displacements at Pombalino building's foundation. Shadings clearly point out the shape of settlements and their influence from the water level drawdown. Figure 4.9 illustrates the evolution of total displacements and their orientation from $x = 48 \text{ m}$ to $x = 70 \text{ m}$ under Pombalino piles. Maximum displacement due to the decrease of water level is computed at the end of phase 5 (figure 4.9 b) and it has a value of $1,81 \text{ mm}$. This is also highlight in figure 4.11: it is shown that displacements induced by water drawdown are parallels and their value increases with the water drawdown. More precisely a total displacement of $0,25 \text{ mm}$ occurs every time that water level decreases by 1 m (figure 4.8). It is also shown that displacement induced by the increase of water table are similar to the ones caused by the third water drawdown.

Figures 4.12 and 4.13 illustrates respectively trends of vertical and horizontal displacements. Parallel lines represent settlements caused by water drawdown and blu line those produced by the activation of Pombalino and parking area. The second one clearly shows the trend discussed about figure 4.6: starting from $x = 55,5 \text{ m}$ horizontal displacements change their orientation toward positive values of coordinate x .

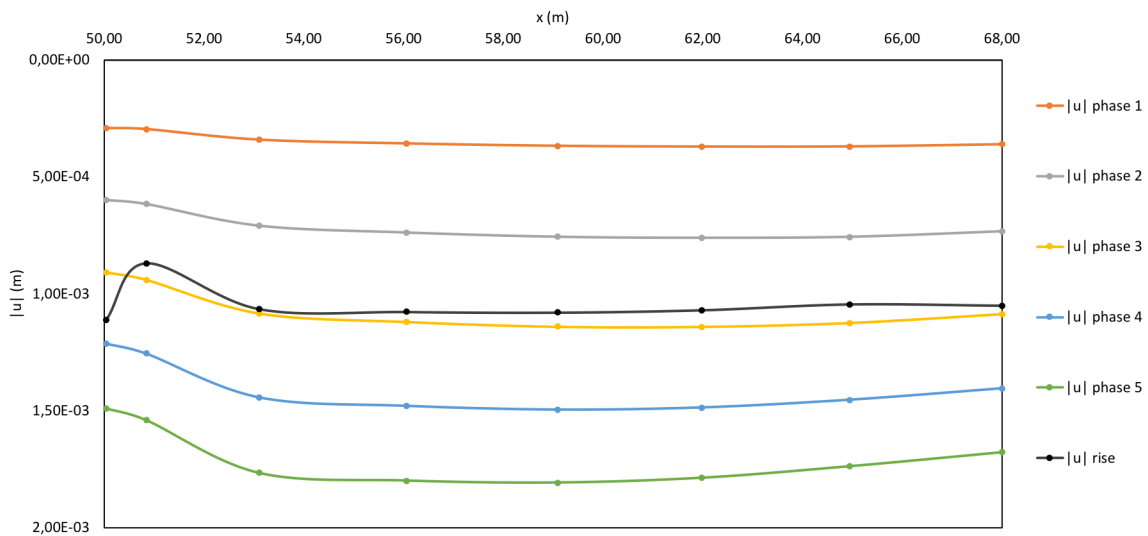


Figure 4.8: Evolution of total displacements induced only by water drawdown under Pombalino building.

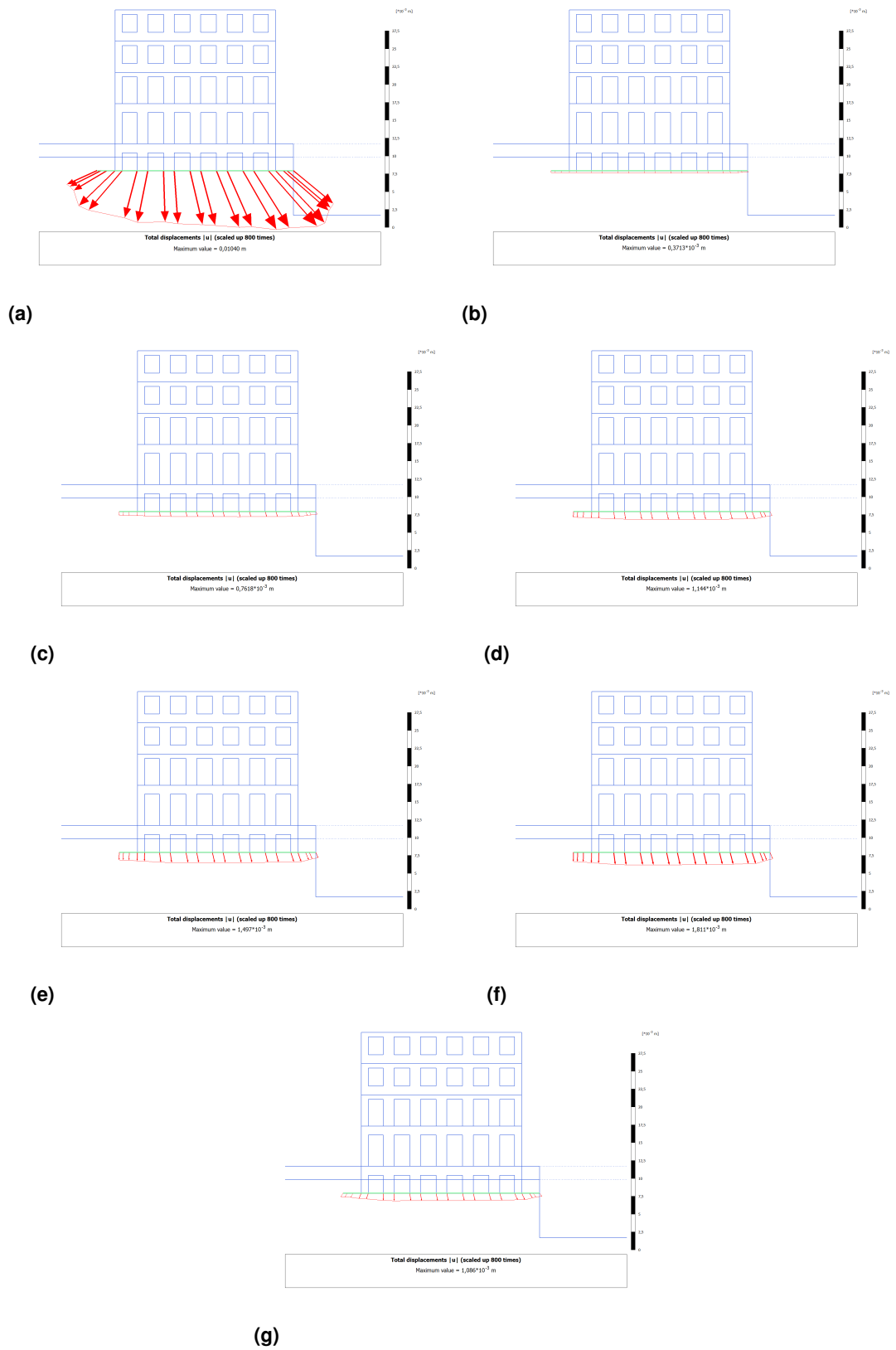


Figure 4.9: Evolution of total displacements under Pombalino building.

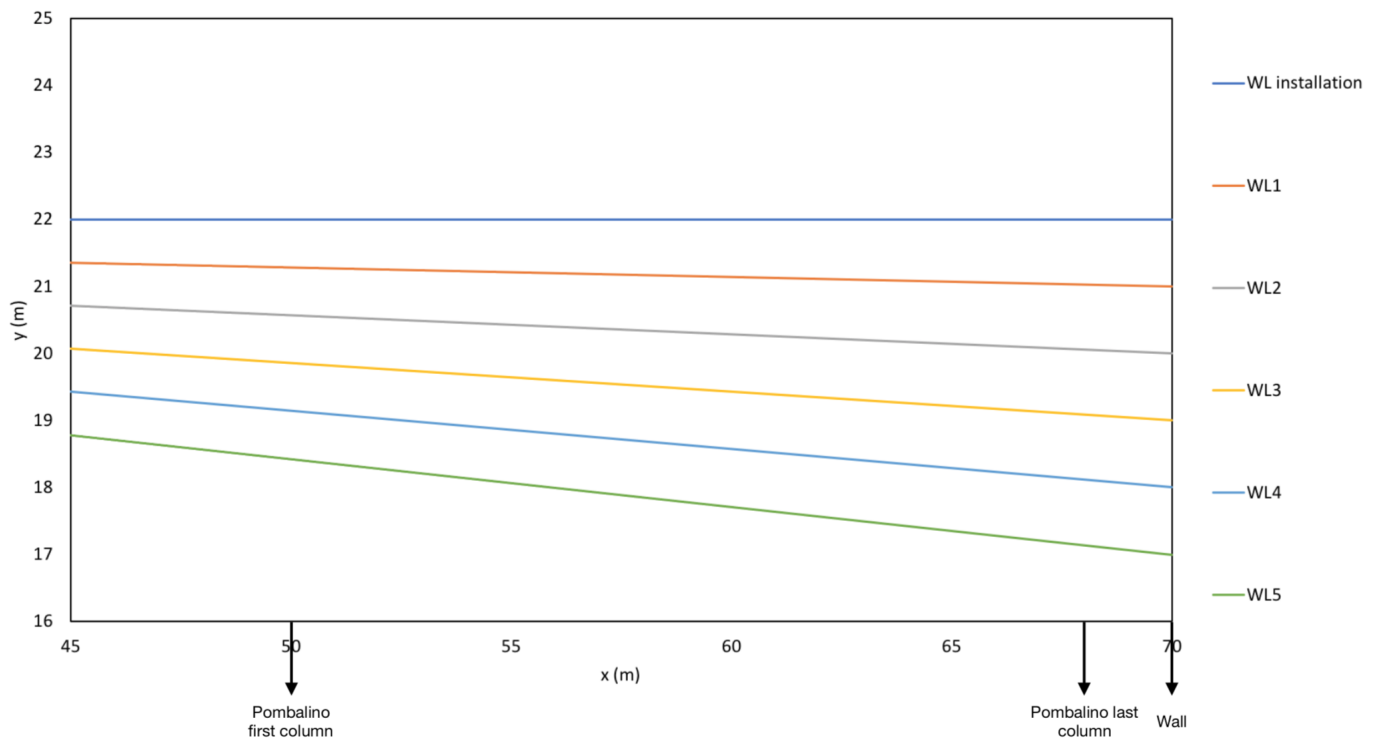


Figure 4.10: Evolution of water drawdown under Pombalino building.

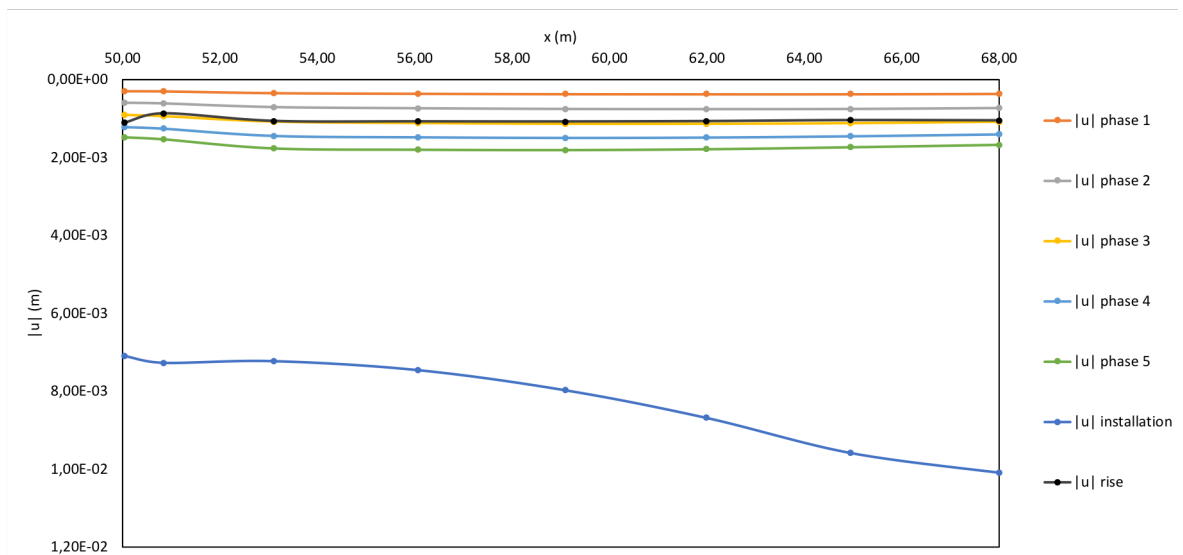


Figure 4.11: Evolution of total displacements under Pombalino building.

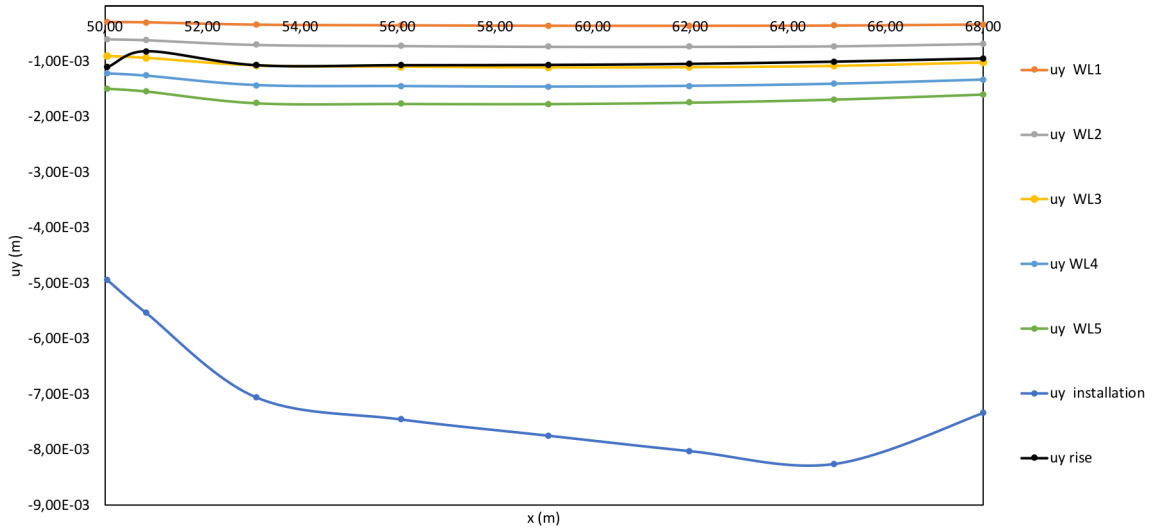


Figure 4.12: Evolution of vertical displacements under Pombalino building.

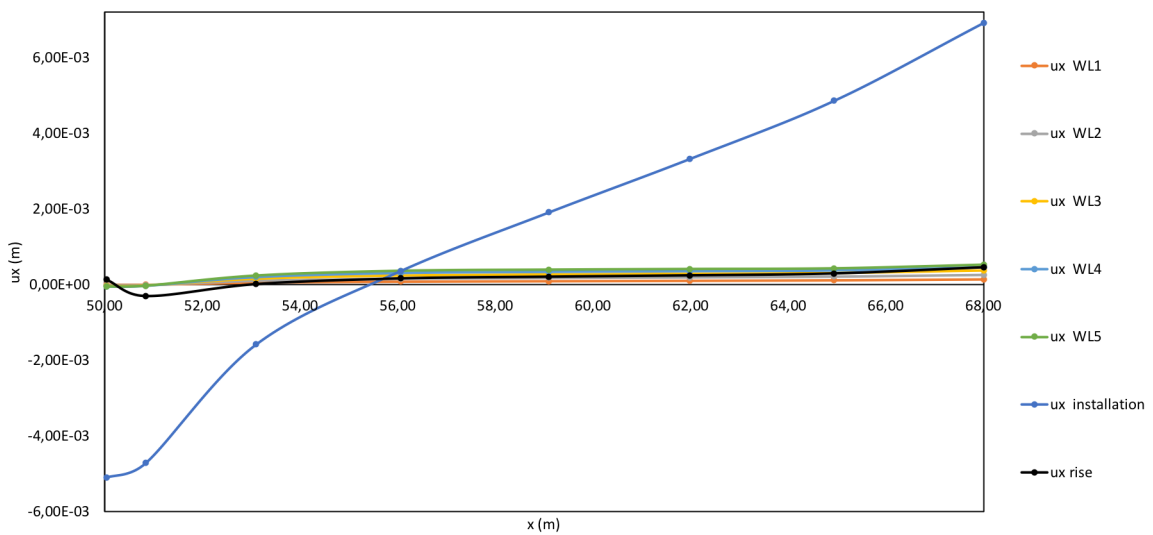


Figure 4.13: Evolution of horizontal displacements under Pombalino building.

To investigate effects of water drawdown on building deformations is possible to focus the attention on ground floor and foundations, upper floors and finally openings. Figure 4.14 shows that deformations thicken in the first column on the left in correspondence of the slab. ε_1 results to be a compressive strain with a maximum value of $-0,61E-3$ and ε_3 is a tensile strain with a maximum value of $0,60E-3$. Comparing deformations with figure 4.17 is noticeable that the first column and slightly also the second tend to rotate clockwise according to deformations shown in figure 4.14.

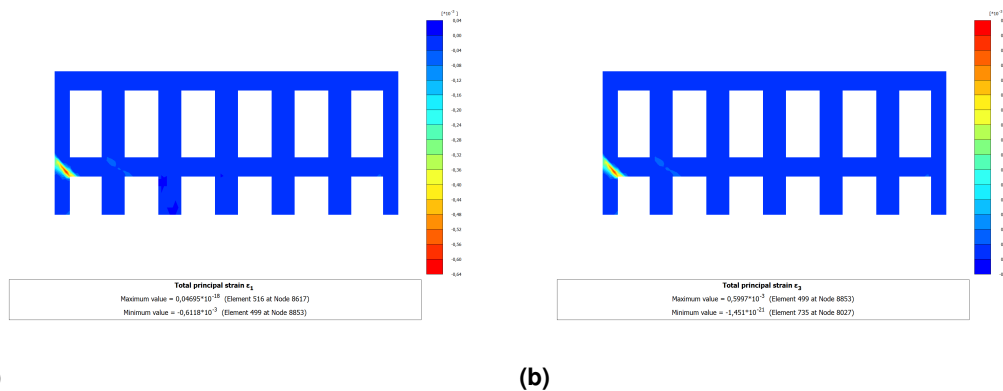


Figure 4.14: Evolution of total strain ε_1 (left) and ε_3 (right) of Pombalino building ground floor at the end of water drawdown.

Figure 4.15 illustrates deformations on the upper floors at the end of water drawdown. ε_1 and ε_3 assume negligible values compared to deformations of ground floor.

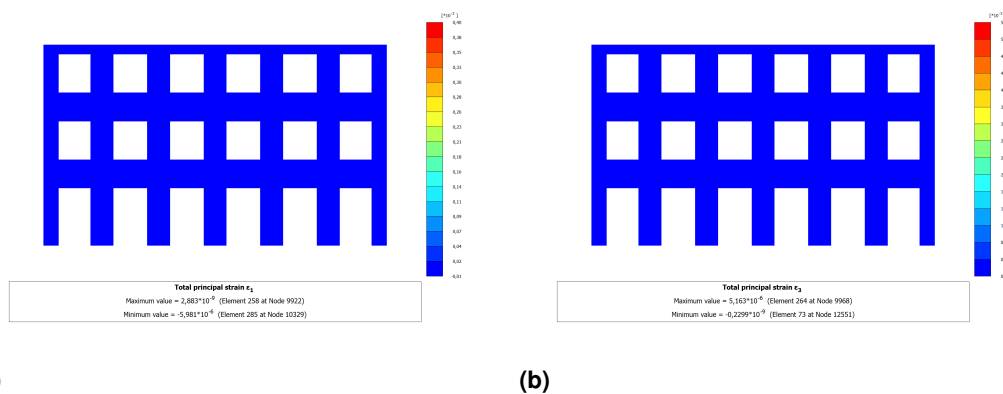


Figure 4.15: Evolution of total strain ε_1 (left) and ε_3 (right) of Pombalino building upper floors at the end of water drawdown.

Finally figure 4.16 shows deformations in the openings of Pombalino building at the end of water level drawdown. Openings at the ground floors are more subjected to deformations. More precisely they have comparable values of ε_1 and ε_3 with a magnitude of $E - 5$. ε_1 behaves as a compression strain and ε_3 as tensile strain. From the first up to the third openings on the left it is evident that deformations follow the weak directions of 45° and 135° selected for the Masonry model. According to the deformed mesh (figure 4.17) the weakest direction of first opening is the one with a dip angle of 135° . The second clearly shows deformations on both weak direction and the third opening presents only the 45° weak direction.

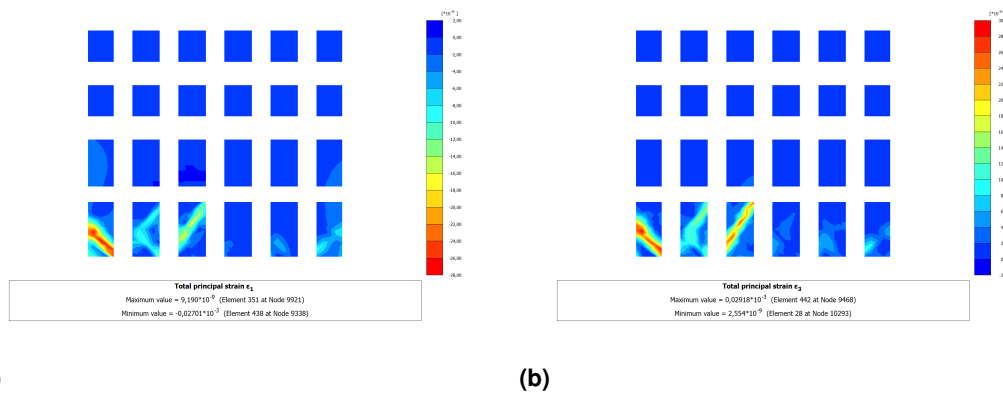


Figure 4.16: Evolution of total strain ε_1 (left) and ε_3 (right) of Pombalino building openings at the end of water drawdown.

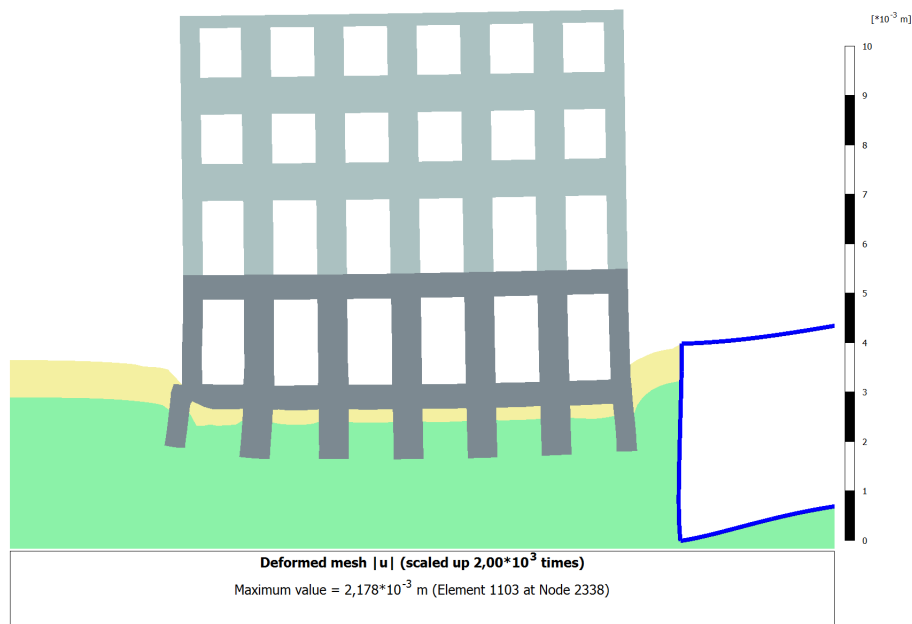


Figure 4.17: The generated deformed mesh for the case study.

Stresses induced by subsidence on buildings at surface are different and often more severe than those caused by settlements related to the self weight of the buildings [13]. Generally damages depend on distortion of the building β , which can be evaluated as the relative rotation of two elements of the structure. It depends on the line displacements geometry, on building length and on its position in relation to the one of line displacement [13].

Boscarding and Cording (1989) analyzed effects of soil distortion and tensile strain on a typical masonry building. The damage is evaluated according to the tensile strain induced on the building [13].

It is possible to focus attention under the first column of Pombalino after the last water table draw-down. Distance between two extreme points of column is $L = 0,80001 \text{ m}$ (computed by PLAXIS 2D) and vertical displacement of last point is $\delta = 1,4E - 3 \text{ m}$. The horizontal strain ε_h is $0,5E - 3$, so, in accordance with equation 4.4, is possible to calculate the angular distortion:

$$\beta = \arcsin \frac{\delta}{L} \quad (4.4)$$

β results equal to 0,1 and according to figure 4.19 is possible to classify the damage as *very slight*.

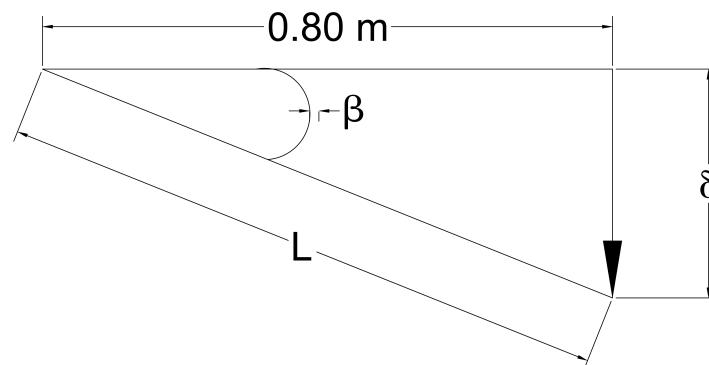


Figure 4.18: Geometry considered to calculate distortion β .

According to table 4.4 is possible to associate a damage category to the limiting tensile strain. For a value of 0,060 of limiting tensile strain, the normal degree of severity corresponds to *Very slight* in accordance with figure 4.19, in the vicinity of a slight damage boundary.

Finally figure 4.20 shows deformations ε_1 , ε_3 and the deformed mesh according to total displacements line at the end of water drawdown. As a conclusion, the water level drawdown can induce *negligible* to *very slight* damage in current Pombalino building.

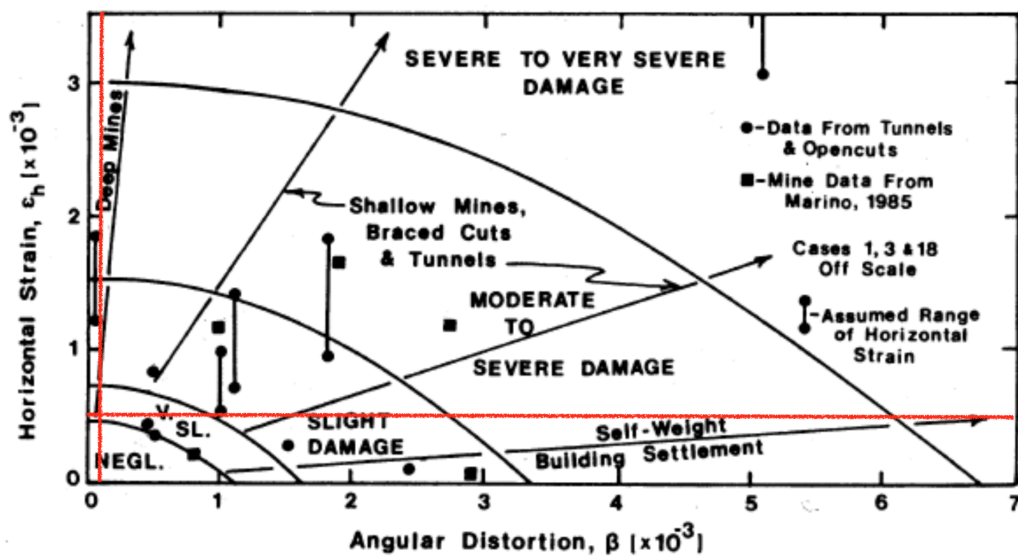


Figure 4.19: Intensity of damage as a function of distortion β and soil extension deformation ε_h (modified by Boscarding & Cording 1989) [13].

Table 4.4: Damage categories associated with the achievement of extension limit deformation in the structure (modified by Boscarding & Cording 1989) [13].

Category of damage	Normal degree of severity	Limiting Tensile strain [%]
0	Negliible	0 - 0,05
1	Very slight	0,05 - 0,075
2	Slight	0,075 - 0,15
3	Moderate	0,15 - 0,3
4 to 5	Severe to Very Severe	>0,3

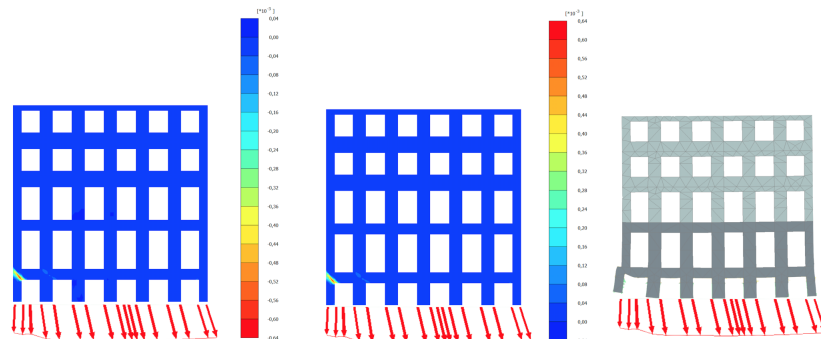


Figure 4.20: From left to right: total strain ε_1 , total strain ε_3 and deformed mesh of Pombalino building in relation to total displacements at the end of water drawdowns.

5

Conclusion

In this thesis the interaction between soil and a typical building situated in Restauradores Square in Lisbon was studied. In the first part a brief geological characterization and a description of Pombalino building were presented. Later basic concepts of numerical models used in the simulation were explained and then results of two numerical tests useful to characterize soil and building behaviour were shown. Finally geometry and properties of the case study were submitted and results were commented.

The aim of this analysis was to evaluate surface displacements and Pombalino deformations induced by the water level drawdown. PLAXIS 2D is the finite element software with which parameters coming from geological surveys and laboratory test were used to simulate soil and structure interaction. Results show that the maximum displacement at the end of water drawdown is $1,81 \text{ mm}$ and effects of surcharge due to the increase of water level are negligible. Pombalino maximum tensile strain is located in the pile farthest from the parking area and its value is $0,61E - 3$ which, according to Boscarding and Cording (1989) [13], corresponds to the damage category *Very slight*.

From this study, it can be concluded that surface settlements cannot be fully explained by water level drawdown. Also, stress relief induced by excavation may play a role. The damages in Pombalino buildings range from small to very slight, also indicating that the damages observed in these buildings cannot be fully explained by water level drawdown.

It would be interesting in the future to analyze the soil-structure interaction taking into account the soil removal simulating as much as possible each excavation phase. Other possible future scenarios are the simulation of a different area with a larger thickness of alluvium deposits and the study of the effects of building's orientation.

Bibliography

- [1] I. R. R. M. C. P. Paula Teves-Costa, Isabel M. Almeida, “Geotechnical characterization and seismic response of shallow geological formations in downtown lisbon,” *Annals of Geophysics*, 2014.
- [2] Meireles, “Seismic vulnerability of pombalino buildings,” Ph.D. dissertation, Instituto Superior Técnico, 2012.
- [3] V. C. Raquel Fernandes Paula, “International workshop on earthquake engineering on timber structures,” in *Rehabilitation of Lisbon’s old “seismic resistant” timber framed buildings using innovative techniques*. University of Coimbra, November 2006.
- [4] M. J. M. D., “A study of the design and construction of buildings in the pombaline quarter of lisbon.” Ph.D. dissertation, Instituto Superior Técnico, 1996.
- [5] R. Catulo, “Análise dinâmica experimental de edifícios de alvenaria e avaliação sísmica de um edifício tipo - definição de base de dados.” Master’s thesis, Instituto Superior Técnico, 2015.
- [6] H. M. C. Renda, “Danos em edifícios de alvenaria provocados por movimentos do terreno,” Master’s thesis, Instituto Superior Técnico, Civil Engineering, June 2016.
- [7] J. M. Mateus, “Reabilitação urbana baixa pombalina: bases para uma intervenção de salvaguarda,” Câmara Municipal de Lisboa, Tech. Rep., 2005.
- [8] J. M. E. D. Cruz, “Avaliação de danos em edifícios pombalinos associados a movimentos do terreno,” Master’s thesis, Instituto Superior Técnico, 2017.
- [9] D. M. Potts and L. Zdravkovic, *Finite element analysis in geotechnical engineering*. Thomas Telford Publishing, Thomas Telford Ltd, 1999.
- [10] B. D. F. M. Lasciarrea, Amorosi, “Jointed masonry model: a constitutive law for 3d soil-structure interaction analysis,” *Engineering Structures*, 2018.
- [11] F. L. J. A. da Silva, “Deformação de estruturas de contenção,” Master’s thesis, Instituto Superior Técnico, Civil Engineering, June 2018.

[12] *Material Model Manual*, PLAXIS, 2016.

[13] D. Boldini, *Dispense del corso di opere in sotterraneo*.

[14] J. G. R. Giorgia Giardina, Max A.N. Hendriks, "Sensitivity study on tunnelling induced damage to a masonry façade," *Engineering Structures*, 2015.

[15] L. G. F. B. João Gomes Ferreira, Ana Maria Gonçalves, "Avaliação do comportamento de paredes em edifícios pombalinos," in *ResearchGate*, April 2011.